UNIVERSITY OF COLORADO BOULDER

Nanoscale Stiffness Cues Influence Valvular Interstitial Cell Activation to Myofibroblasts

AN HONORS THESIS

By

Michaela Ann Wenning

Department of Chemical and Biological Engineering

Department of Biochemistry

Advisor

Kristi S. Anseth, PhD

Department of Chemical and Biological Engineering

Laboratory Mentor

Brian A. Aguado, PhD

Department of Chemical and Biological Engineering

Honors Council Representative

Jeffrey C. Cameron, PhD

Department of Biochemistry

Honors Council Committee Member

Joseph H. Jupille, PhD

Department of Political Science

Defended April 1, 2019

Contents

Abstract

Surgery is currently the primary treatment option for aortic valve stenosis (AVS) patients, many of whom are ineligible for surgery and are left untreated. AVS is progression is known to differ between males and females, and an understanding of sex-specific mechanisms of disease progression is imperative in developing accurate treatment options for men and women. The development of a nonsurgical therapy for AVS patients requires a deeper understanding of the molecular and cellular mechanisms of AVS progression. Currently, the role of calcium phosphate nanoparticles detected in the aortic valve during early stages of AVS in influencing disease progression and valvular interstitial cell (VIC) activation to myofibroblasts is unknown. Here, we sought to characterize the effects of nanoscale stiffness cues on VIC activation to myofibroblasts and hypothesized that alterations in nanoparticle stiffness and size would modulate sex-specific VIC activation and deactivation. Engineered hydrogel cell culture platforms embedded with polystyrene nanoparticles (PS-NPs) of varying size were employed to probe the role of nanoscale stiffness cues in modulating sex-specific VIC activation to the myofibroblast state, while poly(ethylene glycol) (PEG) nanogels of varying stiffness were synthesized and embedded in hydrogels or suspended in VIC media to gain a deeper understanding of VIC response to nanoscale stiffness cues. Analysis of alpha-smooth muscle actin (αSMA) expression and stress fiber formation in VICs in response to nanoscale stiffness cues revealed sex-specific VIC activation and deactivation in response to stiff PS-NPs and PEG nanogels of varying stiffness. Our results support the hypothesis that altering the stiffness and size of nanoparticles might influence sex-specific VIC activation.

Introduction

Aortic valve stenosis (AVS) is a disease that is characterized by fibrosis, calcification, and decreased function of the aortic valve (Carabello et al. 2009). AVS affects more than 12.4% of adults over 75 and progresses rapidly (Osnabrugge et al., 2013), often resulting in heart failure and death within 2-5 years of diagnosis when left untreated (Schlotter et al., 2018). Currently, the primary treatment option for improving survival rates in AVS patients is surgical replacement of the aortic valve, and an effective non-surgical treatment option does not exist (Marquis-Gravel et al., 2016). However, an estimated 30% of patients with severe symptomatic AVS are not eligible for surgery due to risk factors such as age or coexisting conditions (Leon et al., 2010), and a nonsurgical therapy is desired to slow disease progression in these patients. AVS progression begins at the molecular and cellular levels, allowing the disease to go unnoticed until significant damage has been done to the aortic valve (Marquis-Gravel et al., 2016). A specific nonsurgical therapy could target the molecular and cellular mechanisms of AVS progression and halt disease progression in its early stages, but a limited understanding of the molecular mechanisms underlying AVS progression hinders the development of such a treatment. The high mortality rate associated with AVS and lack of nonsurgical treatment options motivate the investigation of the molecular mechanisms that drive AVS progression.

AVS progression has been shown to differ between males and females (Simard et al., 2017). Clinical data suggest that male aortic valves are generally more calcific, while female valves exhibit more fibrosis during AVS progression (Simard et al., 2017). A gene expression analysis of male and female valvular interstitial cells (VICs) suggested that the sexes differ in their ECM organization, calcification, angiogenesis, lipid metabolism, proliferation, and migration during AVS progression (McCoy et al., 2012). The data suggest that male and female valvular cells

experience fundamentally different tissue microenvironments (McCoy et al., 2012 & Simard et al., 2017), and effective nonsurgical therapies must incorporate sex as a variable.

VICs make up the primary fibroblast population in the aortic valve and secrete proteins responsible for maintaining homeostasis to the extracellular matrix (ECM) (Wang et al., 2013). During AVS progression, VICs activate to a myofibroblast phenotype characterized by increased α-smooth muscle actin (αSMA) expression and stress fiber formation (Wang et al., 2013). Several microenvironmental cues are known to influence VIC activation; vascular endothelial growth factor-A (VEGF-A) is thought to regulate the differentiation of myofibroblasts to osteoblasts, while proinflammatory cytokines might stimulate fibrosis and calcification (Weiss et al., 2013). Previous studies reported that VICs activate to the pathogenic myofibroblast phenotype in response to stiff substrates (E > 15 kPa) such as tissue culture polystyrene (TCPS) (E, ~3 GPA) and stiff poly(ethylene glycol) (PEG) hydrogels (E, ~40 kPa), while soft poly(ethylene glycol) (PEG) hydrogels (E, ~7 kPa) inhibit the activation of VICs to myofibroblasts and promote the quiescent VIC phenotype (Wang et al., 2013 & Mabry et al., 2016). Furthermore, the PI3K/AKT pathway is activated in VICs cultured on stiff substrates, and inhibition of the pathway with LY294002 hinders the activation of VICs to myofibroblasts (Wang et al., 2013). Evaluation of PI3K/AKT signaling as a function of sex remains unexplored.

Recently, nanoscale microenvironmental cues have been hypothesized to influence AVS progression (Bertazzo et al., 2013). Stiff nanoscale calcium phosphate nanoparticles of varying size were observed in the ECM of diseased valves, and the role of these stiff particles in AVS progression is not well-understood (Bertazzo et al., 2013). Density-dependent color scanning electron microscopy (DDC-SEM) was used to observe macroscopic calcific lesions in aortic valves, and dense spherical calcium phosphate nanoparticles were present in 100% of the valves

that contained macroscopic calcific lesions (Bertazzo et al., 2013). Furthermore, as disease severity increased, the particle size tended to increase, with particles ranging from 100 nm to 5 μm (Bertazzo et al., 2013). Macroscopic calcific lesions are believed to form from cardiovascular cells such as VICs that differentiate into cells resembling osteoblasts, which yield calcification in the ECM (Bertazzo et al., 2013 & Weiss et al., 2013). Proinflammatory cytokines such as interleukin (IL)-1, IL-17, and interferon-γ produce inflammation that might also contribute to calcification in the aortic valve (Weiss et al., 2013). Calcific lesions have a composition that is very similar to that of bone and contain cells that express genes that are specific to osteoblasts (Weska et al., 2010) and form proteins specific to bone (Rajamannan et al., 2003 & Demer et al., 2008). Notably, dense spherical particles were also observed in 46% of the aortic valves that were thought to be healthy and did not contain macroscopic calcific lesions (Bertazzo et al., 2013). The presence of the spherical nanoparticles in valves without calcific lesions indicates that the particles are the first calcific structure to form in AVS and are likely to influence disease progression. Given that AVS progression differs between males and females, the presence of spherical nanoparticles in the aortic valve leads to open questions as to whether nanoscale stiffness cues in the ECM produce differences in gene expression and VIC activation between male and female VICs.

During cell-particle interactions, nanoparticles interact with cell membrane receptors and recruit clathrin and cytoskeletal proteins to the membrane to form a pit that surrounds the particle (Nel et al., 2009). The reassembly of actin fibers assists with the formation of the pit (Nel et al., 2009). Focal adhesions between cells and the ECM are known to influence gene expression and form when integrins interact with ECM proteins such as fibronectin and recruit cytoskeletal proteins (Pelham et al., 1997), but their role in cell-particle interactions is not well-characterized. The mechanical properties of the cellular environment have been shown to influence the formation

of focal adhesion sites, and stiff substrates have been shown to produce more mature focal adhesions in rat kidney epithelial and 3T3 fibroblastic cells (Pelham et al., 1997). Furthermore, focal adhesions anchor αSMA stress fibers creating high tension required for stress fiber formation, and focal adhesion size has been shown to be positively correlated with αSMA stress fiber formation (Goffin et al., 2006). The sex-specific role of focal adhesion formation in VIC activation to myofibroblasts and αSMA stress fiber formation in response to stiffness cues is not well-understood.

Previous studies have shown that the elasticity of nanoparticles suspended in cell media can impact cell behavior (Liu et al., 2012 & Li et al., 2018). When HepG2 cells were treated with 2-hydroxyethyl methacrylate (HEMA) nanogels of varying stiffness, F-actin organization was altered, and stress fibers were reduced due to the interactions between the nanoparticles and the cell membrane (Liu et al., 2012). All types of particles used in the study influenced the cytoskeletal organization of HepG2 cells, but softer nanogels led to a greater reduction in F-actin stress fiber formation (Liu et al., 2012). Furthermore, the immune response of peripheral blood mononuclear cells (PBMCs) was reduced *in vitro* when PMBCs were treated with hydrophilic nanogels, including PEG nanogels, and *in vivo* when mice induced with lung inflammation were treated with hydrophilic nanogels, decreasing the expression of pro-inflammatory cytokines such as tumor necrosis factor- α (TNF-α) and IL-6 that cause disease (Li et al., 2018). Because treatment with nanogels has been shown to manipulate cell phenotype (Liu et al., 2012) and hinder the mechanisms underlying lung disease (Li et al., 2018), the investigation of VIC response to nanogels of varying stiffness suspended in the media is of interest.

In this thesis, we describe an engineered hydrogel cell culture platform to interrogate the role of nanoscale stiffness cues in modulating the VIC to myofibroblast transition in male and

female cells. We describe the role of nanoscale stiffness cues in modulating VIC activation to myofibroblasts, as well as deactivating myofibroblasts to quiescent VICs. Polystyrene nanoparticles (PS-NPs, E ~ 5.0 GPa) of varying size were embedded in soft PEG hydrogels to recapitulate the nanoscale stiffness cues found in the native valve microenvironment. Upon separating cells by sex, we reveal differences in how male and female VICs activate in the presence of nanoscale stiffness cues presented on the hydrogel surface. PS-NP hydrogels were also used to evaluate sex-specific VIC response to stiff PS-NPs of varying size. To evaluate the sex-specific role of the PI3K/AKT pathway in VIC response to nanoscale stiffness cues, the drug LY294002 was used to inhibit the PI3K/AKT pathway, and sex-specific VIC response to PS-NPs in the presence of the drug was observed. Focal adhesions between VICs and PS-NP hydrogels were visualized and compared to focal adhesions between VICs and blank soft PEG hydrogels to evaluate the role of focal adhesion formation in the interaction of VICs with the PS-NP gels. To further investigate the role of nanoparticle stiffness on VIC activation to myofibroblasts, PEG nanogels of varying PEG weight percent were synthesized. The resulting nanogels were embedded in soft and stiff PEG hydrogels, and the sex-specific response of VICs to the nanogels was evaluated. VICs were also treated with PEG nanogels of varying stiffness suspended in the media, and the activation and deactivation of VICs was compared between males and females. The use of PS-NPs and PEG nanogels in evaluating VIC response to nanoscale stiffness cues *in vitro* provides a strong foundation for evaluating the role of dense spherical calcium-phosphate nanoparticles in AVS progression *in vivo*.

Materials and Methods

PEG Hydrogel Fabrication

Poly(ethylene glycol) (PEG) norbornene (PEG-Nb) was synthesized as described in previous work using 8-arm, 40kDa, amine-functionalized PEG (Aguado et al., 2019 & Fairbanks et al., 2009). To functionalize 12 mm glass coverslips with free thiols, O_2 plasma-treated coverslips were placed in a toluene solution containing 5% vol/vol 2-butylamine and 15% vol/vol mercaptopropyltrimethoxysilane (MPTS, Sigma-Aldrich). 70% ethanol was used to sterilize the thiol-functionalized coverslips prior to cell culture. 8-arm 40 kDa PEG-Nb was mixed with 2 mM CRGDS cell adhesive peptide (Bachem) and 5 kDa PEG-dithiol crosslinker (JenKem) in phosphate buffered saline (PBS, Sigma-Aldrich) at a 0.99:1 thiol-to-ene ratio to create the gel precursor solutions containing 4% or 10% wt/vol PEG-Nb in PBS. Prior to photo-polymerization, the photoinitiator lithium phenyl-2,4,6-trimethylbenzoylphosphinate (LAP) was added to the precursor solution at a concentration of 1.7 mM. Gel precursor solution was UV-photopolymerized on thiol-functionalized coverslips for 3 minutes at 10 mW/cm^2. The resulting PEG hydrogels were sterilized for 30 minutes in 5% isopropyl alcohol in PBS, washed with PBS 3 times and swelled overnight at 37°C and 5% CO_2 in valvular interstitial cell (VIC) media, consisting of Media 199 (Life Technologies), 15% fetal bovine serum (FBS, Life Technologies), 50 U/mL penicillin, 50 µg/mL streptomycin, and 1 µg/mL amphotericin B. To fabricate PEG hydrogels containing polystyrene nanoparticles (PS-NPs, Nanocs), PS-NPs of 200 nm, 500 nm, or 2 µm were added to the gel precursor solution at a concentration of 0.7% solids prior to UV-polymerization. Similarly, PEG hydrogels containing PEG nanogels were fabricated through the addition of PEG nanogels to the gel precursor solution prior to UV-polymerization.

Rheology

Precursor solutions for PEG hydrogels (2% wt/vol PEG-Nb, 4% wt/vol PEG-Nb, 5% wt/vol PEG-Nb, 10% wt/vol PEG-Nb, 20% wt/vol PEG-Nb) were photopolymerized on a HR3 rheometer (TA Instruments) *in situ*, and parallel plate geometry was used to characterize the hydrogel solutions (8 mm diameter). Oscillatory shear rheology with an amplitude of 1% and frequency of 1 Hz were used to make storage (G') and loss (G") measurements. The formula $E = 2G'(1+\nu)$ was used to convert shear modulus values to Young's modulus (E) with $\nu = 0.5$, assuming G' >>> G" (Mabry et al., 2015).

PEG Nanogel Fabrication

PEG nanogels were fabricated using the nanoemulsion technique as previously described (Anselmo et al., 2015). Gel precursor solutions of 2%, 4%, 5%, 6%, 7%, and 10% wt/vol PEG-Nb were prepared by combining 8-arm 40kDa PEG-Nb, 5 kDa PEG-dithiol, 1.7 mM LAP, and 2 mM CRGDS at 0.99:1 thiol-to-ene ratio in PBS. For experiments using nanogels suspended in cell culture media, CRGDS was not added to the gel precursor to prevent VIC detachment from the hydrogel substrate. The aqueous gel precursor solution was added to an oil phase consisting of Span-80 (Sigma) at a dilution of 1:50 and Tween-20 (Sigma) at a dilution of 1:150 in hexanes. The mixture was sonicated (QSonica Q700 Sonicator) on ice for 2 minutes at a setting of 15% of full amplitude, pulsed for 10 seconds at a setting of 30% of full amplitude and allowed to rest for 5 seconds for a total of 4 minutes of sonication, and sonicated again for 2 minutes at a setting of 15% of full amplitude. The emulsified solution was UV-photopolymerized for 3 minutes at 10 mW/cm^2 while being stirred. The resulting nanogels were centrifuged at 18,000g for 10 minutes and resuspended in hexanes 3 times, isopropyl alcohol 3 times, and PBS 3 times. The nanogels were kept in sterile conditions after the first wash with isopropyl alcohol. Nanogel size was recorded

using a Zetasizer (Malvern). Total mass of nanogels was determined by lyophilizing a sample volume and recording the dry mass of solids per volume solution. 300 mg of nanogels were embedded in PEG hydrogels for experiments, while nanogels without CRGDS were suspended at concentrations of 0.22 mg/µL and 0.43 mg/µL.

VIC Isolation and Culture

Valvular interstitial cells (VICs) were harvested from the aortic valve leaflets of porcine hearts as described in a previous study (Aguado et al., 2019). Aortic valve leaflets were rinsed with warmed Earle's Balanced Salt Solution supplemented with 1% Penicillin-streptomycin and 0.5 µg/mL fungizone. The leaflets were incubated for 30 minutes under constant shaking at 5% CO_2 and 37°C in a solution containing 250 units type II collagenase per mL EBSS. Leaflets were vortexed for 30 seconds at maximum speed and incubated under constant shaking for 60 minutes at 5% CO_2 and 37°C in a fresh collagenase solution. Leaflets were again vortexed at maximum speed for 2 minutes. The resulting solution was passed through a 100 µm cell strainer under sterile conditions to collect the cells, which were then centrifuged for 10 minutes at 0.2g. A VIC expansion medium comprised of Media 199 (Life Technologies), 1% penicillin-streptomycin, 0.5 µg/mL fungizone, and 15% FBS (Life Technologies) was used to resuspend the pellets. For expansion, the resulting cells were cultured on tissue culture treated polystyrene (TCPS) at 37°C and 5% CO_2. Trypsin was used to collect VIC cultures after they reached 70-80% confluency, and an automated hemocytometer counted the cells. VICs were seeded in Media 199 (Life Technologies) containing 1% penicillin-streptomycin, 1% FBS (Life Technologies), and 0.5 µg/mL fungizone at 20,000 cells per cm^2 growth area.

Immunostaining

After 72 hours, VICs cultured on PEG hydrogels were fixed by the addition of a solution containing 4% paraformaldehyde in PBS for 20 minutes. 0.1% Triton-X-100 (Fisher Scientific) in PBS was used to permeabilize VICs for 1 hour at room temperature. To prevent non-specific staining, samples were blocked overnight in 5% bovine serum albumin (BSA, Sigma-Aldrich). Cells were incubated with mouse monoclonal anti-αSMA primary antibody (Abcam, clone 1A4, ab7817) at a dilution of 1:200 at room temperature for one hour, washed 3 times with PBS, and incubated in a secondary antibody solution comprised of HCS Cell Mask (Life Technologies) at a dilution of 1:5000 (according to manufacturer specifications), goat anti-mouse Alexa Fluor 488 (Life Technologies) at a dilution of 1:300, and 4'-6-diamidino-2-phenyindole (DAPI, Life Technologies) at a dilution of 1:500. To image and quantify VIC activation, samples transferred to a glass-bottom 24 well plate (Cellvis) imaged with an Operetta high-content confocal microscope sing a 20x objective, and Harmony software (Perkin Elmer) used αSMA intensity values normalized to DAPI intensity values to automatically counted VICs containing αSMA stress fibers. For each condition, 3 gel replicates were performed, and 5 fields of view were quantified per gel. To stain for focal adhesions, rabbit monoclonal anti-paxillin (Abcam, clone Y113, ab32084) was added to the primary antibody solution at a dilution of 1:400, and goat anti-rabbit Alexa Fluor 647 (Life Technologies) was added to the secondary antibody solution at a dilution of 1:200. Focal adhesions were imaged at the BioFrontiers Institute Advanced Light Microscopy Core. Laser scanning confocal microscopy was performed on a Nikon A1R microscope supported by NIST-CU Cooperative Agreement award number 70NANB15H226. The focal adhesion area was measured using ImageJ (Utku et al., 2014 & Ma et al., 2017). The background was subtracted using the sliding paraboloid option and a rolling ball radius of 50 pixels

(Utku et al., 2014). The paxillin stain was thresholded and made binary, and the area of focal adhesions was calculated with the Analyze Particles function (Utku et al., 2014 & Ma et al., 2017). VICs were considered activated if they expressed αSMA stress fibers.

Statistical Analysis

For each experiment, 3 biological replicates were performed, and 5 images per biological replicate were quantified. For focal adhesions, 20 cells were analyzed per biological replicate. Data are presented as the mean ± standard deviation. One-way ANOVA was used, and significance was claimed at $p < 0.05$. Tukey post-tests were used for multiple comparisons in Prism 8 (Graphpad Software, Inc).

Results

VIC activation to myofibroblasts increases with increasing concentration of 200 nm PS-NPs embedded in soft hydrogels

Due to the increasing concentration of dense spherical particles observed in the aortic valve during AVS progression (Bertazzo et al., 2013), we hypothesized that VICs would activate to myofibroblasts in the presence of stiff nanoparticles. To test this hypothesis, we seeded VICs on soft 4% PEG hydrogels containing PS-NPs of 200 nm diameter at varying concentrations. PS-NPs of 200 nm diameter were embedded in soft 4% PEG hydrogels at particle concentrations of 0.01%, 0.02%, 0.05%, 0.1%, and 0.2% solids, without altering the bulk modulus of the hydrogel (Figures 1A & 2B, provided by Brian Aguado). Soft 4% PEG hydrogels without PS-NPs were used as the negative control (Figure 2A, provided by Brian Aguado), while transforming growth factor beta 1 (TGFβ1), a compound known to upregulate αSMA expression in VICs (Gould et al., 2012), was used as the positive control. We observed VIC activation increased as the concentration of 200 nm PS-NPs embedded in the hydrogel increased (Figure 3A). VIC activation did not increase in response to 0.01% solids 200 nm PS-NPs, but activation significantly increased with each two-fold increase in PS-NP concentration thereafter (Figure 3B) (Soft Control: 40.94 ± 0.11%. TGFβ1 Control: 64.42 ± 1.06%. +0.01% NPs: 41.53 ± 0.43%. +0.02%: 45.74 ± 0.80%. +0.05% NPs: 50.71 ± 0.81%. +0.1% NPs: 53.31 ± 0.54%. +0.2% NPs: 59.64 ± 1.65%).

VIC activation to myofibroblasts increases when 500 nm PS-NPs are embedded in soft hydrogels at high concentrations

After observing the ability of VICs to respond to nanoscale stiffness cues in the form of increasing concentrations of 200 nm PS-NPs embedded in soft hydrogels, we investigated the effect of nanoparticle size on VIC activation. Dense spherical particles observed in the aortic valve

during disease progression vary in size (Bertazzo et al., 2013), so we hypothesized that increasing the concentration of PS-NPs of 500 nm diameter would also increase VIC activation. PS-NPs of 500 nm diameter were embedded in soft 4% PEG hydrogels at varying concentrations without significantly changing the bulk modulus of the hydrogel (Figures 1B & 2C, provided by Brian Aguado). Soft 4% PEG hydrogels without PS-NPs were used as the negative control, while TGFβ1 was used as the positive control. VICs activated in response to 0.05% and 0.2% 500 nm PS-NPs but remained deactivated on hydrogels containing 0.01%, 0.02%, and 0.1% 500 nm PS-NPs (Figure 4A, B) (Soft Control: 40.94 ± 0.11%. TGFβ1 Control: 64.42 ± 1.06%. +0.01% NPs: 43.23 ± 0.04%. +0.02%: 44.82 ± 0.50%. +0.05% NPs: 49.44 ± 1.02%. +0.1% NPs: 42.99 ± 3.92%. +0.2% NPs: 56.21 ± 1.96%)

Inhibition of the PI3K/AKT pathway decreases male VIC activation in response to nanoscale stiffness cues

Given the observation that VICs activate in response to stiff PS-NPs, we next sought to characterize the signaling pathways involved in mediating VIC activation in response to nanoscale stiffness cues. The PI3K/AKT pathway is known to be involved in VIC activation to the myofibroblast state in response to stiff hydrogel substrates and tissue culture polystyrene (TCPS) (Wang et al., 2013). As such, we hypothesized the PI3K/AKT pathway might also mediate myofibroblast activation in response to polystyrene nanoparticles. We tested male VIC activation on soft 4% PEG hydrogels embedded with 200 nm, 500 nm, and 2,000 nm PS-NPs in the presence or absence of LY294002 (10 μM), a small molecule inhibitor of the PI3K/AKT pathway (Wang et al., 2013). Dimethyl sulfoxide (DMSO) was used at a concentration of 10 μM in the control conditions.

Male VIC activation in response to 200 nm PS-NPs was inhibited by LY294002 ($p < 0.0001$), with activation decreasing from 73.69 ± 9.40% to 51.61± 8.63% in the presence of the inhibitor (Figure 5A, B). Activation on gels containing 500 nm PS-NPs was also significantly decreased by LY294002 ($p = 0.0259$), with an activation 65.20 ± 8.86% without the inhibitor and an activation of 51.22 ± 10.03% with the inhibitor (Figure 5B). The inhibitor also decreased male VIC activation on hydrogels containing 2000 nm PS-NPs ($p = 0.0062$), with activation decreasing from 56.73 ± 8.82% to 41.81 ± 10.63% (Figure 5B). Additionally, male VIC activation was observed to decrease with increasing PS-NP size (Figure 5A, B). Male VIC activation was significantly decreased on gels containing 2000 nm PS-NPs compared to gels containing 200 no PS-NPs ($p = 0.001$) (Figure 5B). Furthermore, all conditions treated with LY294002 were not significantly different from the blank control, which had an activation of 42.48 ± 12.11%, or the blank control with the inhibitor, which had an activation of 53.21 ± 15.05% (Figure 5B).

Inhibition of the PI3K/AKT pathway does not influence female VIC activation in response to PS-NPs

Acknowledging that AVS has sexually dimorphic outcomes (Simard et al., 2107 & McCoy et al., 2012), we next investigated potential sex differences in VIC response to nanoparticles and tested female VIC response to LY294002 and PS-NPs of varying size. We hypothesized that female VICs would have reduced activation responses to nanoscale stiffness cues because female patients experience less calcification in the aortic valve during AVS progression (Simard et al., 2017). To determine the role of the PI3K/AKT pathway in female VIC response to nanoscale stiffness cues, female VICs were seeded on soft 4% PEG hydrogels embedded with 200 nm, 500 nm, and 2,000 nm PS-NPs, and blank 4% PEG hydrogels were used as negative controls. Female VICs were treated with LY294002 or DMSO at a concentration of 10 μM in the media.

We observed VIC activation to be significantly higher on stiff 10% PEG hydrogel controls ($p < 0.0001$) and on gels containing 200 nm PS-NPs ($p = 0.0004$), 500 nm PS-NPs ($p = 0.0224$), and 2,000 nm PS-NPs ($p < 0.0001$) (Figure 6A, B). Female VIC activation in the presence of LY294002 on stiff 10% PEG hydrogel control decreased to 55.58 ± 9.89% from 86.33 ± 5.71% activation on stiff hydrogel controls ($p < 0.0001$) (Figure 6B). On soft hydrogels containing 200 nm PS-NPs, VIC activation was statistically similar ($p = 0.7817$) between cells treated without (69.16 ± 8.95%) and with (61.70 ± 8.22%) LY294002 inhibitor (Figure 6B). Female VIC activation also did not change on gels containing 500 nm PS-NPs when treated without (67.46 ± 11.10%) and with (57.43 ± 12.31%) LY294002 inhibitor ($p = 0.4251$) (Figure 6B). On gels containing 2,000 nm PS-NPs, female VICs did not respond to the inhibitor, with similar activation levels at 81.72 ± 7.07% without the inhibitor and 79.14 ± 9.10% with the inhibitor ($p > 0.9999$) (Figure 6B). Of note, VIC activation levels on 2,000 nm PS-NP gels with or without inhibitor were statistically similar to stiff hydrogel controls without PI3K/AKT inhibition (Figure 6B). With respect to particle size, female VIC activation was significantly greater on gels containing 2,000 nm PS-NPs than gels containing 200 nm PS-NPs ($p = 0.0449$) and gels containing 500 nm PS-NPs ($p = 0.0412$) (Figure 6B).

Focal adhesion size does not change in male VICs in response to PS-NPs

Because focal adhesions are known to form when cells interact with stiff substrates and influence αSMA stress fiber formation (Pelham et al., 1997 & Goffin et al., 2006), we next investigated the effect of nanoscale stiffness cues on focal adhesion maturation. Focal adhesions were analyzed by staining for paxillin, a protein involved in the formation of focal adhesion complexes (Ma at al., 2017 & Zamir et al., 2000). Given that αSMA stress fiber formation in male VICs increases on PS-NP hydrogels, we hypothesized that focal adhesions would be larger in male

VICs on PS-NP hydrogels and might play a role in VIC activation. However, analysis of focal adhesion size on soft hydrogels and PS-NP hydrogels revealed that focal adhesion size is not changed when VICs are seeded on PS-NP hydrogels ($p > 0.1$ for all comparisons) (Figure 7). The mean focal adhesion size was 3.31 ± 0.83 μm^2 on the soft control, 3.58 ± 1.06 μm^2 on gels containing 200 nm PS-NPs, 3.74 ± 1.10 μm^2 on gels containing 500 nm PS-NPs, and 3.36 ± 1.16 μm^2 on gels containing 2,000 nm PS-NPs.

Nanogels of varying stiffness were developed via suspension polymerization

After establishing a role for nanoscale stiffness cues in mediating VIC activation via the PI3K/AKT pathway, we next sought to develop nanoparticles with tunable mechanical properties to explore VIC response to nanoscale stiffness cues. Using a suspension polymerization technique (Anselmo et al., 2015), we generated PEG nanogels of varying PEG weight percent (2 wt%, 4 wt%, 5 wt%, 6 wt%, 7 wt%, and 10 wt%). Data of the bulk modulus of PEG hydrogels of varying PEG weight percent suggest that PEG nanogel stiffness increases with increasing PEG weight percent (Figure 8, provided by Brian Aguado). Using dynamic light scattering, we determined the z-average diameter of PEG (Figure 9 A: 2% PEG nanogels. Z-average diameter = 391 nm. B: 4% PEG nanogels. Z-average diameter = 307 nm. C: 5% PEG nanogels. Z-average diameter = 329 nm. D: 6% PEG nanogels. Z-average diameter = 203 nm. E: 7% PEG nanogels. Z-average diameter = 378 nm. F: 10% PEG nanogels. Z-average diameter = 380 nm. G: 4% PEG nanogels without RGD. Z-average diameter = 325 nm. H: 10% PEG nanogels without RGD. Z-average diameter = 318 nm).

Male VICs have reduced activation on stiff hydrogels embedded with soft nanogels

Using nanogels of tunable stiffness, we next characterized male VIC response to soft nanogels by seeding VICs on stiff 10% PEG hydrogels embedded with soft 4% PEG nanogels. We

hypothesized male VICs would interact with soft nanogels and deactivate in response. 300 mg of soft 4% PEG nanogels were embedded in each hydrogel, and male VIC activation was determined (Figure 10A). Soft 4% PEG hydrogels were used as a negative control, while stiff 10% PEG hydrogels were used as a positive control.

Male VICs were deactivated on stiff 10% PEG hydrogels embedded with soft 4% PEG nanogels (60.44 ± 13.31% activation) when compared to the stiff control (73.74 ± 11.96% activation) ($p = 0.0260$) (Figure 10B). Furthermore, the percent activation on the nanogel-containing gels was not significantly different from the soft control (59.74 ± 17.20% activation) ($p > 0.9999$) (Figure 10B).

Female VICs remain activated as myofibroblasts on stiff hydrogels embedded with soft nanogels

Female VICs were also seeded on stiff 10% PEG hydrogels embedded with soft 4% PEG nanogels to investigate the sex-specific response to soft 4% PEG nanogels. We hypothesized that female VICs would respond to the soft nanoscale stiffness cues similarly to male VICs and deactivate in response to the soft 4% PEG nanogels. 300 mg of soft 4% PEG nanogels were embedded in each hydrogel, and female VIC activation was determined (Figure 11A). Soft 4% PEG hydrogels were used as a negative control, while stiff 10% PEG hydrogels were used as a positive control.

Unlike male VICs, female VICs activated on stiff 10% PEG hydrogels embedded with soft 4% PEG nanogels (87.60 ± 8.83% activation) when compared to the soft control (59.90 ± 9.33% activation) ($p < 0.0001$). The percent activation on the nanogel-containing gels was not significantly different from the stiff control (93.69 ± 4.14% activation) ($p = 0.6991$) (Figure 11B). Female VICs were significantly more activated than male VICs on both the stiff 10% PEG

hydrogel control ($p = 0.0001$) and the stiff 10% PEG hydrogels embedded with soft 4% PEG nanogels ($p < 0.0001$) (Figures 10B & 11B).

Male VIC activation increases when nanogels of increasing stiffness are embedded in soft hydrogels

To further elucidate the role of nanogel stiffness on VIC activation, male VICs were seeded on soft 4% PEG hydrogels embedded with PEG nanogels of 2, 4, 5, 6, 7, or 10 PEG wt%. We hypothesized that male VIC activation would increase on the soft 4% PEG hydrogels as the stiffness of the PEG nanogels embedded in the hydrogel increased from the softest nanogel (2 PEG wt%) to the stiffest nanogel (10 PEG wt%). Blank 4% PEG hydrogels and 4% PEG hydrogels embedded with 200 nm PS-NPs were used as controls. Male VICs were used because they responded to soft 4% PEG nanogels embedded in the hydrogel, while female VICs did not respond to nanogels embedded in the hydrogel.

Male VIC activation increased as nanogel stiffness increased in the soft 4% PEG hydrogels (Figure 12A, B) (Control: 43.94 ± 7.51%. +2% PEG nanogels: 37.73 ± 8.92%. +4% PEG nanogels: 46.56 ± 8.58%. +5% PEG nanogels: 52.50 ± 9.89%. +6% PEG nanogels: 59.48 ± 8.42%. +7% PEG nanogels: 67.26 ± 7.89%. +10% PEG nanogels: 73.79 ± 7.64%. +200 nm PS-NPs: 84.07 ± 8.87%). VIC activation on the blank 4% PEG hydrogel control was not significantly different from gels containing 2% PEG nanogels ($p = 0.4584$), 4% PEG nanogels ($p = 0.9875$), or 5% PEG nanogels ($p = 0.0887$) (Figure 12B). Activation on gels containing 2% PEG nanogels was significantly less than activation on gels containing 5% PEG nanogels ($p < 0.0001$), while activation on gels containing 4% PEG nanogels was not significantly different from activation on gels containing 5% PEG nanogels ($p = 0.0887$) but was significantly less than activation on gels containing 6% PEG nanogels ($p < 0.0001$) (Figure 12B). Furthermore, VIC activation on gels

containing 5% PEG nanogels was not significantly different from activation on gels containing 6% PEG nanogels ($p = 0.2107$) but was significantly less than activation on gels containing 7% PEG nanogels ($p < 0.0001$) (Figure 12B). On gels containing 6% PEG nanogels, VIC activation did not differ from activation on gels containing 7% PEG nanogels ($p = 0.0792$) but was significantly less than activation on gels containing 10% PEG nanogels ($p < 0.0001$) (Figure 12B). Similarly, VIC activation on gels containing 7% PEG nanogels was not significantly different from VIC activation on gels containing 10% PEG nanogels ($p = 0.2606$) but was significantly less than activation on gels containing 200 nm PS-NPs ($p < 0.0001$) (Figure 12B). Gels containing 200 nm PS-NPs resulted in significantly more VIC activation than any other gels, including gels containing 10% PEG nanogels ($p = 0.0135$) (Figure 12B).

Male VIC activation decreases when nanogels of decreasing stiffness are embedded in stiff hydrogels

Male VICs were then seeded on stiff 10% PEG hydrogels embedded with PEG nanogels of 2, 4, 5, 6, 7, or 10 PEG wt% to further characterize the interaction between male VICs and nanogels. We hypothesized that male VICs would deactivate on the stiff 10% PEG hydrogels as the stiffness of the PEG nanogels embedded in the hydrogel decreased from the stiffest nanogel (10 PEG wt%) to the softest nanogel (2 PEG wt%).

Male VIC activation tended to decrease as nanogel stiffness decreased in the stiff 10% PEG hydrogels (Figure 13A, B) (Stiff 10% PEG hydrogel control: 71.50 ± 7.88%. +200 nm PS-NPs: 85.27 ± 6.67%. +10% PEG nanogels: 72.00 ± 19.40%. +7% PEG nanogels: 77.87 ± 4.93%. +6% PEG nanogels: 69.63 ± 6.14%. +5% PEG nanogels: 71.45 ± 5.84%. +4% PEG nanogels: 64.00 ± 10.45%. +2% PEG nanogels: 58.41 ± 7.97%). Male VIC activation on the stiff 10% PEG hydrogel was not significantly different from activation on gels containing 200 nm PS-NPs ($p = 0.2229$),

10% PEG nanogels ($p > 0.9999$), 7% PEG nanogels ($p > 0.9999$), 6% PEG nanogels ($p > 0.1053$) but was significantly greater than activation on gels containing 5% PEG nanogels ($p = 0.0108$), 4% PEG nanogels ($p < 0.0001$), and 2% PEG nanogels ($p < 0.0001$) (Figure 13B). Furthermore, activation on gels containing 200 nm PS-NPs was not significantly different from stiff gels containing 10% PEG nanogels ($p = 0.1472$) or 7% PEG nanogels ($p = 0.0840$) but was significantly greater than activation on stiff gels containing 6%, 5%, 4%, and 2% PEG nanogels ($p < 0.0001$) (Figure 13B). Activation on stiff gels containing 10% PEG nanogels was not significantly different from activation on gels containing 7% PEG nanogels ($p > 0.9999$) or 6% PEG nanogels ($p = 0.0862$) but was significantly greater than activation on stiff gels containing 5% PEG nanogels ($p = 0.0052$), 4% PEG nanogels ($p < 0.0001$), and 2% PEG nanogels ($p < 0.0001$) (Figure 13B). Male VIC activation on stiff gels containing 6% PEG nanogels was not significantly different from VIC activation on stiff gels containing 5% PEG nanogels ($p > 0.9999$) or 4% PEG nanogels ($p = 0.6497$) but was significantly greater than activation on stiff gels containing 2% PEG nanogels ($p = 0.0043$) (Figure 13B). On stiff gels containing 5% PEG nanogels, male VIC activation did not differ from activation on stiff gels containing 4% PEG nanogels ($p = 0.2904$) but was greater than activation on stiff gels containing 2% PEG nanogels ($p < 0.0001$) (Figure 13B). Male VIC activation on stiff gels containing 4% PEG nanogels did not differ from activation on stiff gels containing 2% PEG nanogels ($p = 0.3467$) (Figure 13B).

Male and female VIC activation decreases when treated with suspended soft nanogels and increases when treated with suspended stiff nanogels

To further validate the role of nanoscale stiffness cues in manipulating VIC phenotype, we also treated VICs with nanogels suspended in cell culture media. We hypothesized that male VIC activation would increase in the presence of stiff nanogels suspended in the media and decrease in

the presence of soft nanogels suspended in the media. In contrast, we posited female VICs would not respond to nanogels suspended in the media, given that female VICs did not respond to nanogels embedded in the PEG hydrogel network. Male and female VICs were seeded on stiff 10% PEG hydrogels and treated with soft 4% PEG nanogels at concentrations of 0.22 mg/μL and 0.43 mg/μL. Male and female VICs were also seeded on soft 4% PEG hydrogels and treated with stiff 10% PEG nanogels at concentrations of 0.22 mg/μL and 0.43 mg/μL. To mimic the treatment of VICs that experience nanoscale pockets of stiffness in the aortic valve, male and female VICs were also seeded on soft 4% PEG hydrogels embedded with stiff 200 nm PS-NPs and treated with soft 4% PEG nanogels at a concentration of 0.43 mg/μL. Control samples were not treated with nanogels.

Male VIC activation decreased from 71.50 ± 7.88% on stiff 10% PEG hydrogels to 59.47 ± 9.21% and 60.80 ± 9.14% when treated with 0.22 mg/μL ($p = 0.0026$) and 0.43 mg/μL ($p = 0.0107$) of soft 4% PEG nanogels, respectively (Figure 14A, C). Increasing the concentration of nanogels did not significantly change male VIC activation ($p = 0.9993$) (Figure 14C). Similarly, female VIC activation decreased from 69.20 ± 7.46% on stiff 10% PEG hydrogels to 53.53 ± 13.13% and 58.21 ± 6.87% when treated with 0.22 mg/μL ($p = 0.0003$) and 0.43 mg/μL ($p = 0.0346$) of soft 4% PEG nanogels, respectively (Figure 14B, D). Increasing the concentration of nanogels did not significantly change female VIC activation ($p = 0.8938$) (Figure 14D).

When treated with 0.43 mg/μL stiff 10% PEG nanogels, male VIC activation increased from 51.92 ± 6.20% on the soft 4% PEG hydrogel control to 70.00 ± 9.30% ($p = 0.0011$) (Figure 14C). Similarly, female VIC activation increased from 51.87 ± 10.18% on the soft 4% PEG hydrogel control to 67.80 ± 10.11% and 63.00 ± 9.94% when treated with 0.22 mg/μL ($p = 0.0004$) and 0.43 mg/μL ($p = 0.0402$) of stiff 10% PEG nanogels, respectively (Figure 14D). Again,

increasing the concentration of nanogels did not significantly change activation ($p = 0.8707$) (Figure 14D).

Furthermore, male and female VIC activation decreased on soft 4% PEG hydrogels embedded with 200 nm PS-NPs when treated with 0.43 mg/μL soft 4% PEG nanogels (Figure 14C, D). Male VIC activation decreased from 77.14 ± 6.64% to 63.00 ± 8.26% on gels containing PS-NPs when treated with soft 4% PEG nanogels ($p = 0.0012$), while female VIC activation decreased from 76.00 ± 10.16% to 62.56 ± 8.41% under the same conditions ($p = 0.0049$) (Figure 14C, D).

Discussion

This thesis describes a new role for nanoscale stiffness cues in mediating valvular interstitial cell activation to pro-fibrotic myofibroblasts. Numerous reports suggest a myriad of mechanical and biochemical cues from the valvular tissue microenvironment influence VIC phenotype and partially mediate myofibroblast activation over time. Biochemical cues, such as vascular endothelial growth factor-A (VEGF-A) and proinflammatory cytokines secreted from inflammatory immune cells, promote the activation of VICs to myofibroblasts, which eventually cause microenvironmental stiffening during AVS progression (Weiss et al., 2013). After observing that healthy valve tissue contains nanoscale calcium phosphate particles that increase in size and density during AVS progression (Bertazzo et al., 2013), we posited nanoscale stiffness cues might regulate myofibroblast activation. We engineered hydrogels embedded with stiff PS-NPs to explore the potential role of nanoscale stiffness cues in mediating VIC activation. As a proof of concept, we used commercially available PS-NPs as a tool to demonstrate that mechanosensitive VICs simultaneously respond to bulk modulus, nanoscale stiffness, and nanoparticle size to activate to a myofibroblast state. While soft poly(ethylene glycol) (PEG) hydrogels are known to maintain fibroblast quiescence (Wang et al., 2013 & Mabry et al., 2016), we demonstrated the incorporation of stiff nanoparticles, without altering the bulk modulus of the hydrogel, activate VICs to myofibroblasts. Our results implicate that naturally occurring nanoscale stiffness cues in the valve tissue microenvironment might promote myofibroblast activation in valvular tissue.

After observing VIC activation in response to stiff PS-NPs embedded in the hydrogel network, we postulated VIC activation in response to nanoscale stiffness cues might be a function of nanoparticle stiffness. For a more comprehensive investigation of the role of nanoscale stiffness cues in VIC activation, we developed PEG nanogels of varying stiffness through the adaptation of

a nano-emulsion technique (Anselmo et al., 2015) for PEG norbornene (PEG-Nb) chemistry. PEG nanogels allowed for the modulation of nanoscale stiffness cues embedded in the hydrogel network, providing a more complete platform for understanding the role of nanoscale stiffness cues on VIC activation *in vitro* than PS-NPs alone. Furthermore, previous studies have shown treatment of cells with suspended nanogels modulates cytoskeletal organization (Liu et al., 2012) and hinders disease-causing cellular activity (Li et al., 2018). We hypothesized treatment of VICs with suspended nanogels might modulate αSMA stress fiber formation and VIC activation. As such, we treated VICs seeded on substrates with varying mechanical properties with nanogels of varying stiffness optimized for suspension in VIC media to demonstrate VIC interaction between bulk modulus and nanogel stiffness present in suspension.

AVS progression is known to differ between males and females, with clinical data showing that male aortic valves are more calcific, while female aortic valves are more fibrotic (Simard et al., 2017). On the cellular level, male and female VICs are known to differ in gene expression (McCoy et al., 2012). We sought to probe potential sex-specific VIC responses to nanoscale stiffness cues and posited male and female VICs would have unique responses to PS-NPs and nanogels of varying stiffness. Throughout our investigation, we elicited sex-specific responses to nanoscale stiffness cues presented to VICs in various ways. We demonstrated that male VIC activation decreases with increasing PS-NP size and is strongly regulated by the PI3K/AKT pathway, while female VIC activation increases with increasing PS-NP size and is not strongly regulated by the PI3K/AKT pathway. Our study is in agreement with numerous studies that have reported NPs to alter cytoskeletal organization in cells (Lie et al., 2012, Pernodet et al., 2006, Vieira et al., 2017, Pati et al., 2016, Garcia-Hevia et al., 2016, Wu et al., 2010, & Gupta et al.,

2004), but the mechanisms underlying the ability of NPs to alter cytoskeletal organization are not well-understood (Septiadi et al., 2018).

Given that αSMA stress fiber formation is known to be regulated by VIC focal adhesion formation with the extracellular matrix (ECM) (Goffin et al., 2006 & Ma at al., 2017), we hypothesized VIC activation in response to PS-NPs is regulated by focal adhesion formation. After comparing focal adhesion size in VICs on soft hydrogels to VICs on PS-NP hydrogels, we discovered the average focal adhesion size per cell is not changed by the presence of PS-NPs in the hydrogel and is not likely to be involved in increased VIC activation in response to PS-NPs. However, the average focal adhesion size under all conditions was considered to be mature (1 to 5 μm^2) (Yang et al., 2016 & Chen et al., 1997), indicating that focal adhesion formation likely played a partial role in VIC activation. After observing that focal adhesion size is mature but not changed by the presence of PS-NPs, we hypothesized that NPs bind to cell membrane receptors that trigger VIC activation (Shang et al., 2014 & Nel et al., 2009). Shang et al. reported that smaller NPs are able to recruit more cell membrane receptors to trigger a strong cell-particle interaction (2014), which is consistent with our observation that male VIC activation decreases with increasing PS-NP size. However, our discovery that female VIC activation increases as PS-NP size increases is not consistent with the same hypothesis, as it appears that female VICs form stronger interactions with larger PS-NPs. β1 integrins on VICs, which are known to bind to fibronectin type III repeats in CRGDS (Chi-Rosso et al., 1997) and transforming growth factor-β1 (TGFβ1), stimulate αSMA stress fiber formation when bound (Cushing et al., 2005). We believe β1 integrins are involved in VIC interactions with PS-NPs, and we suggest that female VICs express more β1 integrins and therefore are able to interact more strongly with larger particles than male VICs, which will require future validation. We propose that male VICs are able to bind more

tightly to smaller 200 nm PS-NPs than 2,000 nm PS-NPs because male VICs are able to recruit enough receptors to surround the 200 nm PS-NPs, while the 2,000 nm PS-NPs are too large for sufficient recruitment of receptors. Furthermore, we observed male VIC activation to alter in response to nanogels embedded in the hydrogel, while female VIC activation remained unchanged. This result implies interaction between male VICs and nanoscale stiffness cues was stronger than the interaction between male VICs and the bulk stiffness of the hydrogel, while female VICs interacted more strongly with the bulk stiffness of the hydrogel. We propose β1 integrins on male VICs preferentially bind to nanogels due to their small size, leaving few β1 integrins to interact with the stiff hydrogel. Female VICs might also preferentially bind to nanogels, but if they express many β1 integrins, then a significant number of β1 integrins are left to bind to the hydrogel and respond to the bulk stiffness of the hydrogel. However, we observed both male and female VICs to respond to suspended nanogels. We postulate suspended nanogels are more readily available to the VIC cell membrane receptors than embedded nanogels, allowing more VIC β1 integrins to preferentially interact with suspended nanogels than embedded nanogels and leaving few β1 integrins to interact with the bulk stiffness of the hydrogel. Therefore, our hypothesis that female VICs express more β1 integrins than male VICs is consistent with our results. However, future work should include characterization of β1 integrin expression in male and female VICs.

In this thesis, we characterized the role of nanoscale stiffness cues in the differentiation of VICs to myofibroblast, but VICs are also known to transdifferentiate to osteoblasts, which produce calcification in the ECM and are characterized by increased expression of the osteoblast marker Runx2 (Weiss et al., 2013 & Wang et al., 2015). As AVS is a fibro-calcific disease, future work in evaluating the role of nanoscale stiffness cues on the sex-specific osteogenic differentiation of VICs through the quantification of Runx2 expression might provide valuable insight to effects of

nanoscale stiffness cues on valvular calcification. Furthermore, our work was limited by the use of PS-NPs over calcium phosphate NPs. While PS-NPs might mimic the stiffness of calcium phosphate nanoparticles present in the valve (Bertazzo et al., 2013), the material itself might influence VIC activation, and future work should evaluate the role of calcium phosphate NPs on VIC differentiation to myofibroblasts. Additionally, our inability to directly characterize the stiffness of PEG nanogels leaves open questions regarding our ability to modulate nanogel stiffness. Future work should consider techniques to measure nanogel stiffness; a continuous microfluidic device has been used to measure the viscoelastic properties of hydrogel microparticles in previous studies (Niu et al., 2018) and might be a good candidate for measuring the stiffness of our PEG nanogels. Furthermore, our sample size limits the scope of our study, as we have noted variability in gene expression between harvested batches of VICs. Future work should evaluate the effect of nanoscale stiffness cues across multiple batches of VICs.

The understanding of sex-specific mechanisms of AVS progression is critical in developing therapies for the accurate treatment of men and women with AVS. While some sex-specific characteristics of AVS progression are known (Simard et al., 2017 & McCoy et al., 2012), our analysis of sex-specific responses to nanoscale stiffness cues sheds light on important differences in VIC behavior between male and female patients. The improvement of engineered *in vitro* models of disease using more accurate biomaterials might lead to future advancements in the understanding of the role of nanoscale stiffness cues in modulating disease progression and lead to future drug discovery.

Conclusion

AVS progression begins at the molecular and cellular level, and a deeper understanding of the sex-specific mechanisms that drive disease progression is required to develop an accurate treatment for male and female AVS patients. The research presented here describes the ability of nanoscale stiffness cues to mediate sex-specific VIC activation to the diseased myofibroblast state. We demonstrated the ability of PS-NPs embedded in the hydrogel network to activate male and female VICs, without changing the bulk modulus of the hydrogel, and elicited sex-specific responses to PS-NPs of varying size, with male VIC activation decreasing with increasing particle size and female VIC activation increasing with increasing particle size. We evaluated the role of the PI3K/AKT pathway in VIC response to PS-NPs and demonstrated that the PI3K/AKT pathway regulates male VIC activation in response to PS-NPs but does not regulate female VIC activation in response to PS-NPs. Furthermore, the presence of PS-NPs in the hydrogel does not influence VIC focal adhesion size. Given the ability of PS-NPs to alter VIC phenotype, we developed PEG nanogels of varying stiffness to further probe VIC response to nanoscale stiffness cues. Upon embedding soft nanogels in a stiff hydrogel network, we discovered male VICs deactivated in response to soft nanogels, while female VICs remained activated in response to the bulk stiffness of the hydrogel. Furthermore, male VIC activation increased as nanogel stiffness increased in soft and stiff hydrogels. When treated with suspended nanogels, both male and female VICs activated in response to stiff suspended nanogels and deactivated in response to soft suspended nanogels. Together, these *in vitro* studies describe the ability of nanoscale stiffness cues to manipulate the phenotype of mechanosensitive VICs and provide a platform for understanding the sex-specific role of calcium phosphate nanoparticles in AVS progression, which might lead to future development of targeted therapies to hinder AVS progression.

Figures

Figure 1: Bulk modulus of soft PEG hydrogels does not change when PS-NPs are embedded in the hydrogel network. (A) Soft gels embedded with 200 nm PS-NPs. (B) Soft gels embedded with 500 nm PS-NPs. (C) Soft gels embedded with 2,000 nm PS-NPs. Figure provided by Brian Aguado.

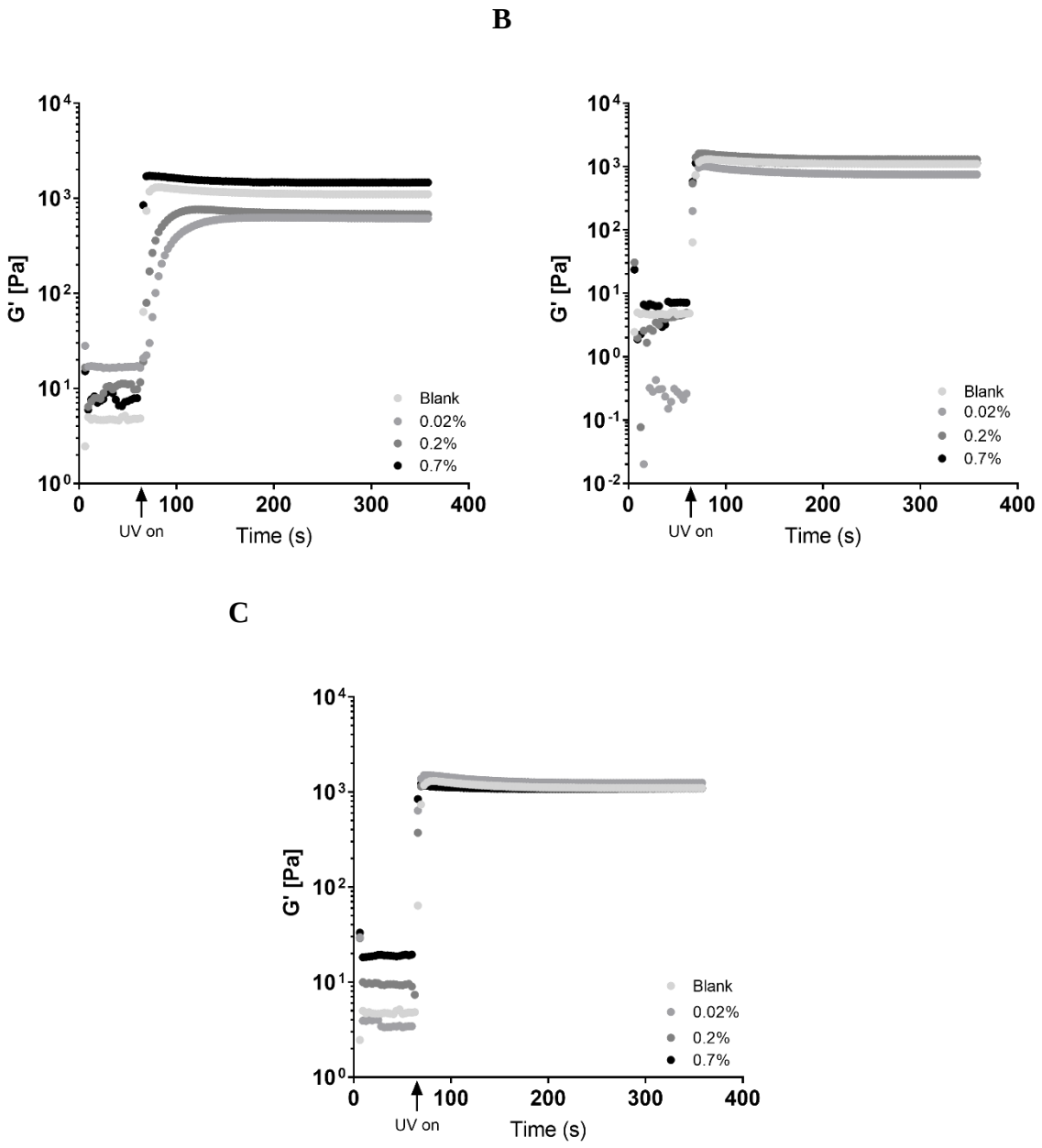

Figure 2: SEM reveals gel topography of soft 4% PEG hydrogels containing PS-NPs of varying size. (A) Blank 4% PEG hydrogel. (B) 4% PEG hydrogel embedded with 200 nm PS-NPs. (C) 4% PEG hydrogel embedded with 500 nm PS-NPs. (D) 4% PEG hydrogel embedded with 2,000 nm PS-NPs. Scale bar: 5 μm. Figure provided by Brian Aguado.

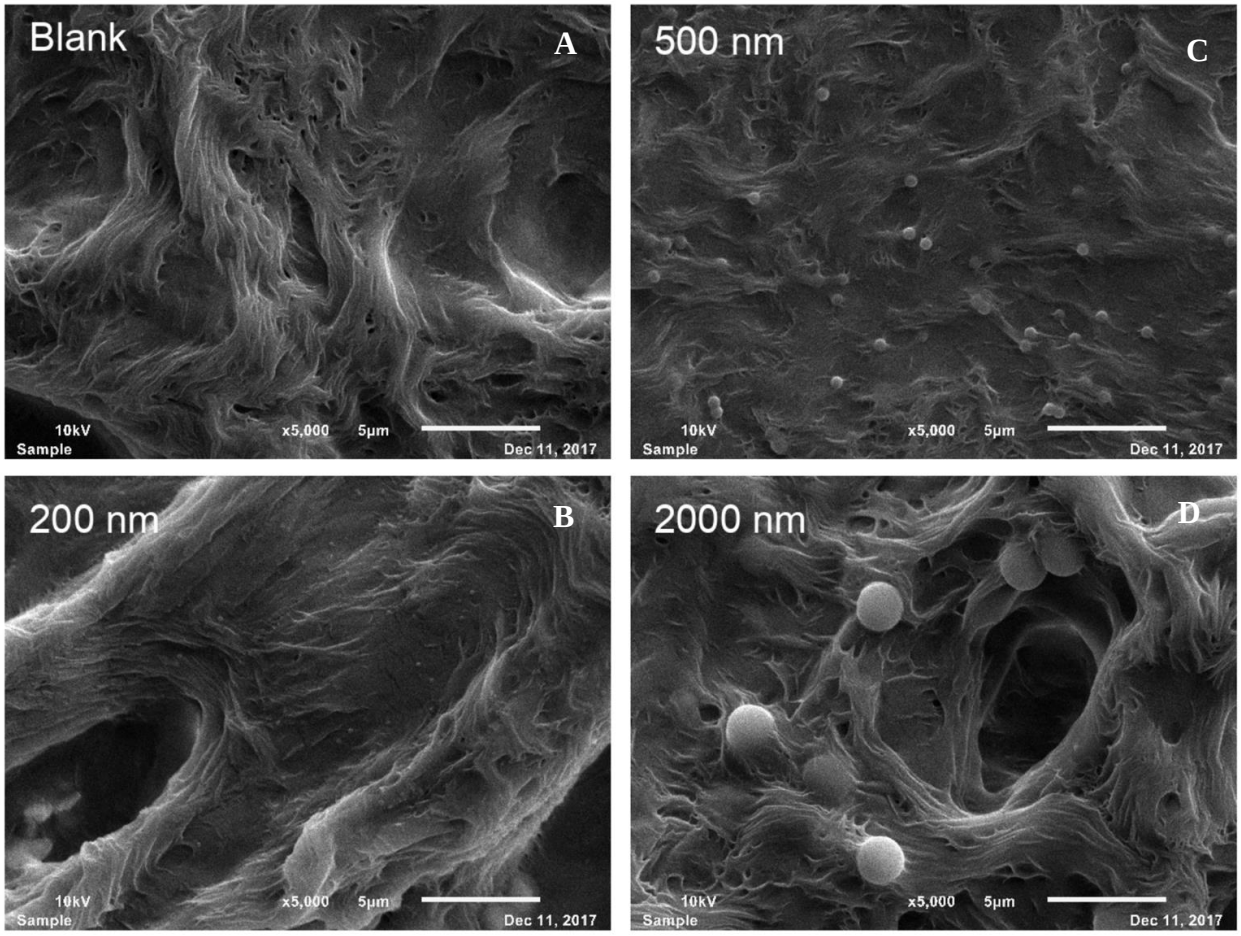

Figure 3: VIC activation increases as the concentration of 200 nm PS-NPs embedded in soft 4% PEG hydrogels increases. (A) Representative images of VICs seeded on soft 4% PEG hydrogels containing 200 nm PS-NPs. Stains: green = αSMA, red = cytoplasm, blue = nuclei. Scale bar = 100 μm. (B) VIC activation in response to increasing concentrations of 200 nm PS-NPs. Sample size: n = 3 gels. Groups with different letters indicate statistical significance (p < 0.05). Figure provided by Brian Aguado.

A

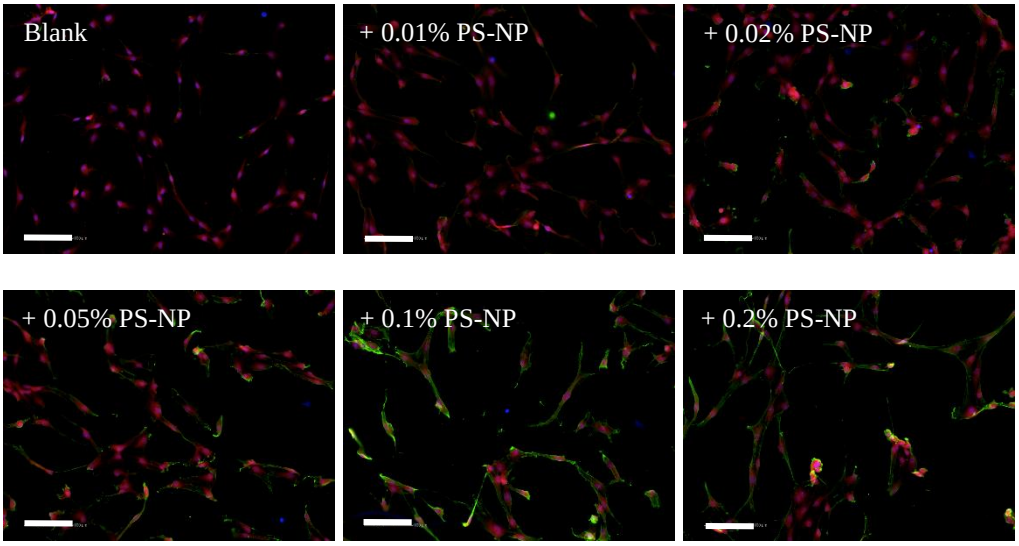

B

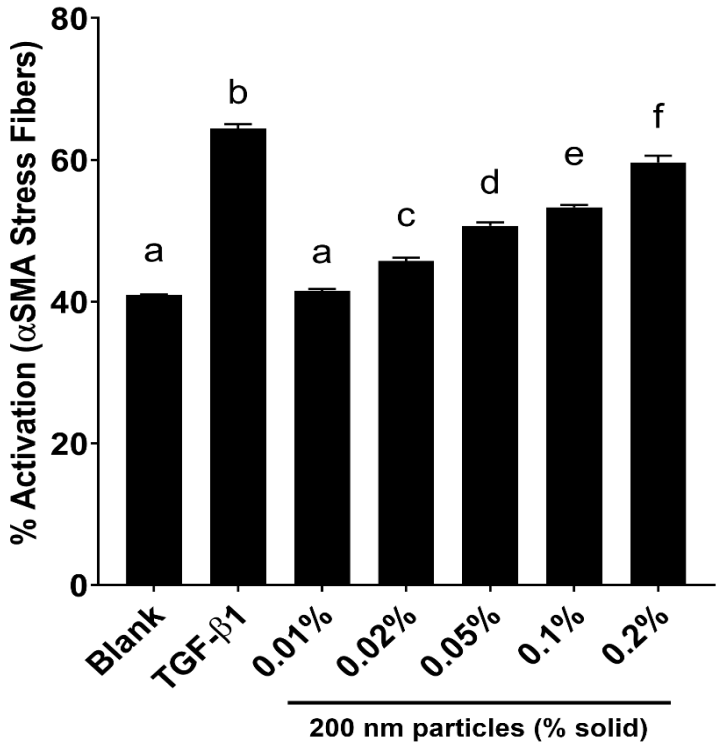

Figure 4: VIC activation increases as the concentration of 500 nm PS-NPs embedded in soft 4% PEG hydrogels increases. (A) Representative images of VICs seeded on soft 4% PEG hydrogels containing 500 nm PS-NPs. Stains: green = αSMA, red = cytoplasm, blue = nuclei. Scale bar = 100 μm. (B) VIC activation in response to increasing concentrations of 500 nm PS-NPs. Sample size: n = 3 gels. Groups with different letters indicate statistical significance (p < 0.05). Figure provided by Brian Aguado.

A

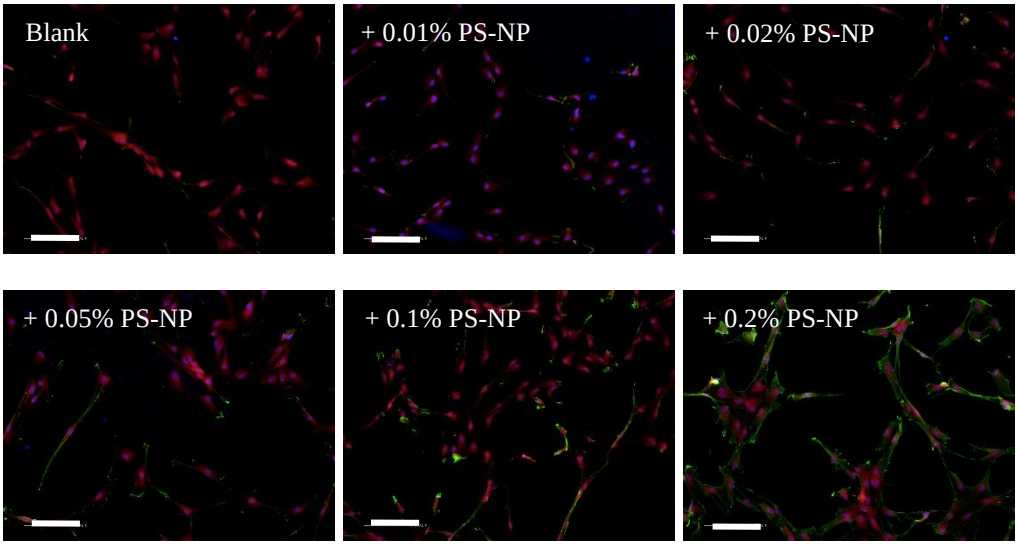

B

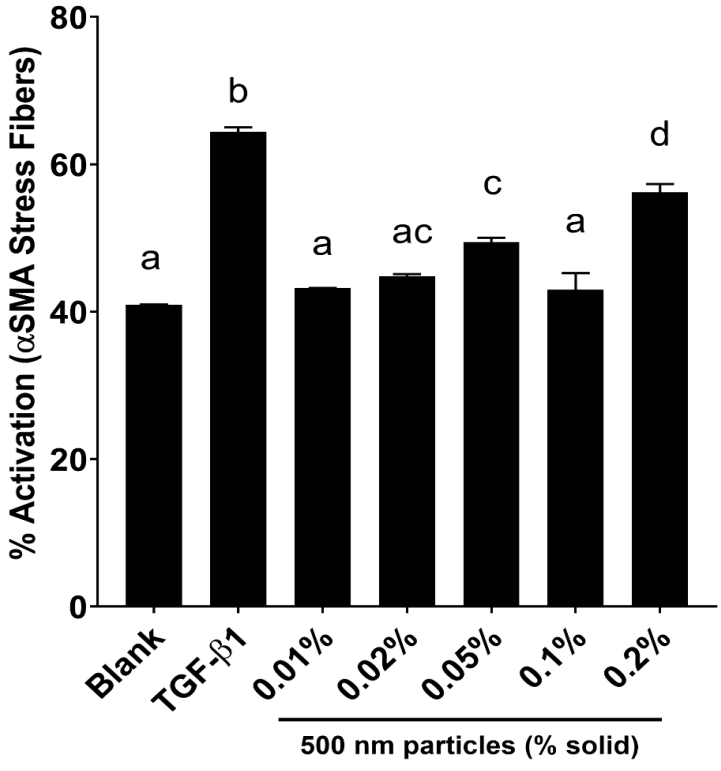

Figure 5: Male VIC activation decreases in response to LY294002 on soft hydrogels embedded with 200 nm and 2,000 nm PS-NPs. (A) Representative images of male VICs seeded on soft 4% PEG hydrogels containing PS-NPs and treated with 10 μM DMSO or LY294002. Stains: green = αSMA, red = cytoplasm, blue = nuclei. Scale bar = 100 μm. (B) Male VIC activation in response to LY294002 and PS-NPs of varying size. Sample size: $n = 3$ gels. Groups with different letters indicate statistical significance ($p < 0.05$).

A

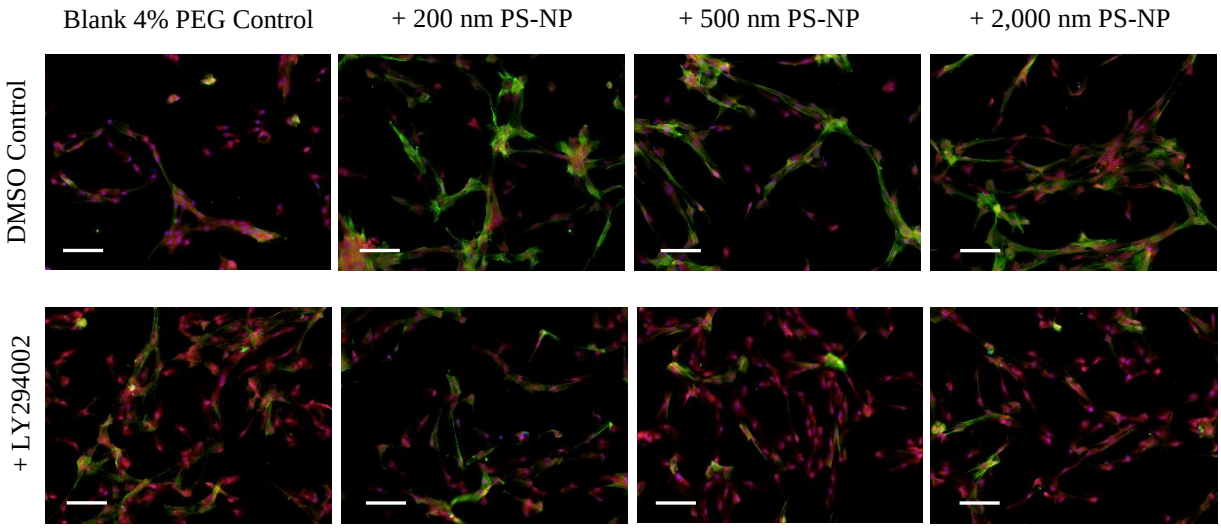

B

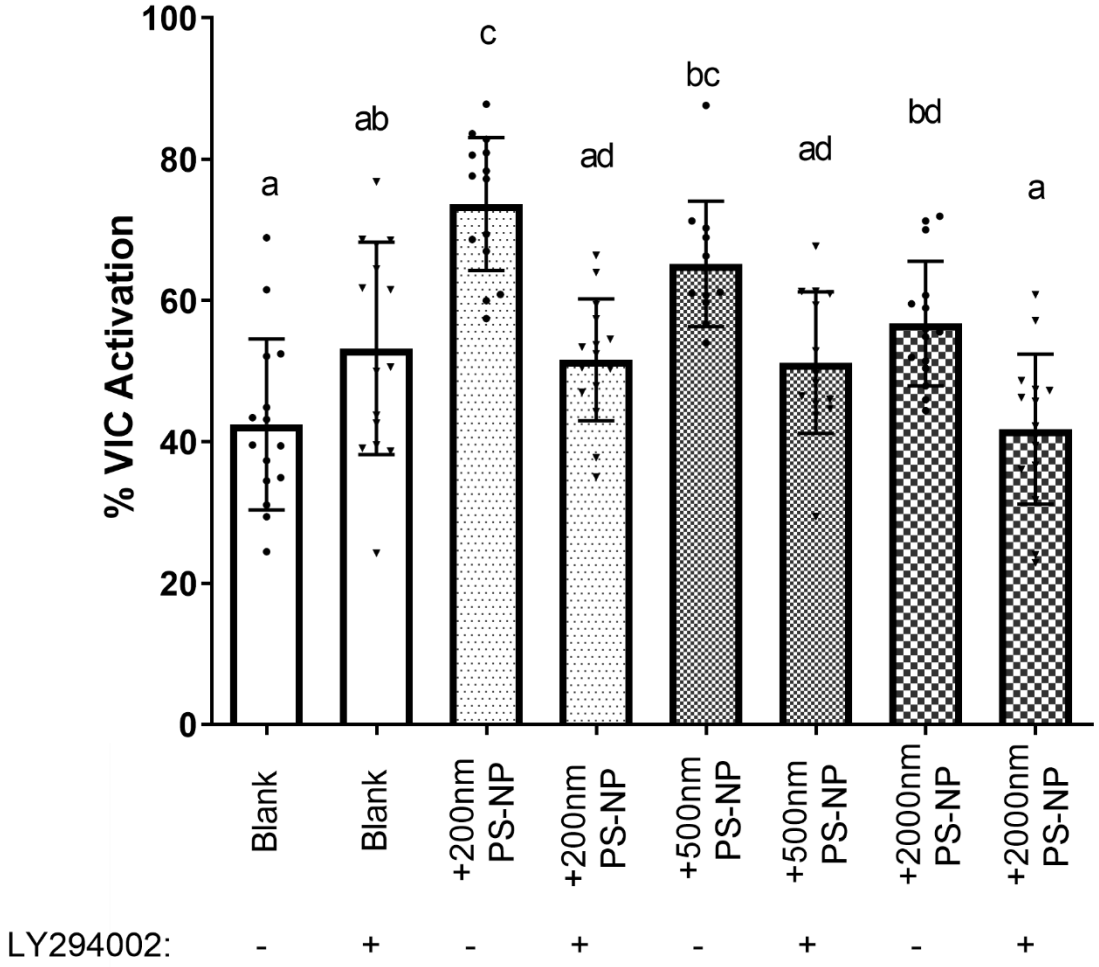
% VIC Activation
100
80
60
40
20
0
a
ab
c
ad
bc
ad
bd
a
Blank
Blank
+200nm PS-NP
+200nm PS-NP
+500nm PS-NP
+500nm PS-NP
+2000nm PS-NP
+2000nm PS-NP
LY294002: - + - + - + - +

Figure 6: Female VIC activation is not changed by LY294002 on soft hydrogels embedded with 200 nm, 500 nm, or 2,000 PS-NPs but decreases on stiff hydrogels when treated with LY294002. (A) Representative images of female VICs seeded on soft 4% PEG hydrogels containing PS-NPs or stiff 10% PEG hydrogels and treated with DMSO or LY294002. Stains: green = αSMA, red = cytoplasm, blue = nuclei. Scale bar = 100 μm. (B) Female VIC activation in response to LY294002 and PS-NPs of varying size. Sample size: $n = 3$ gels. Groups with different letters indicate statistical significance ($p < 0.05$).

A

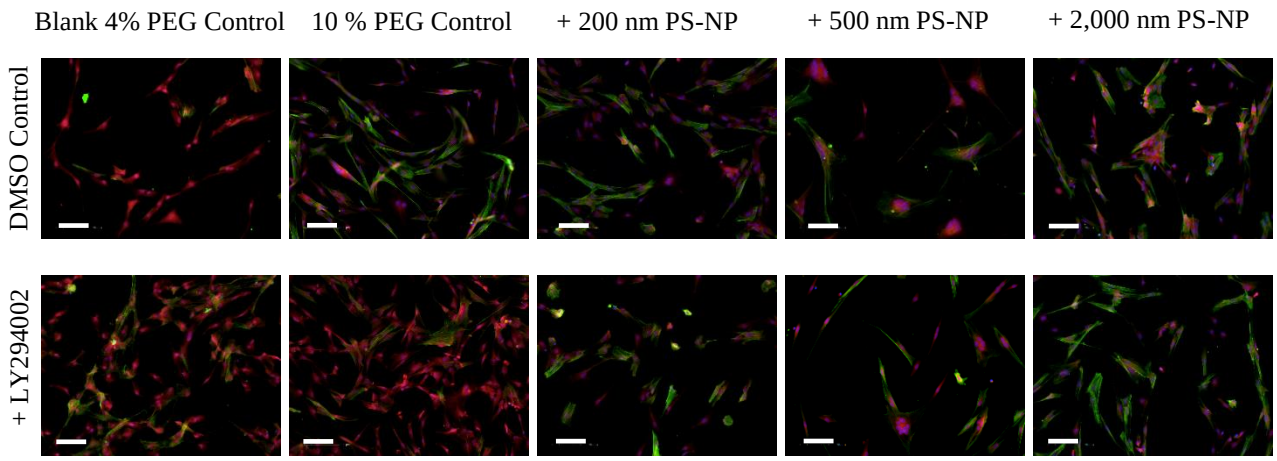

B

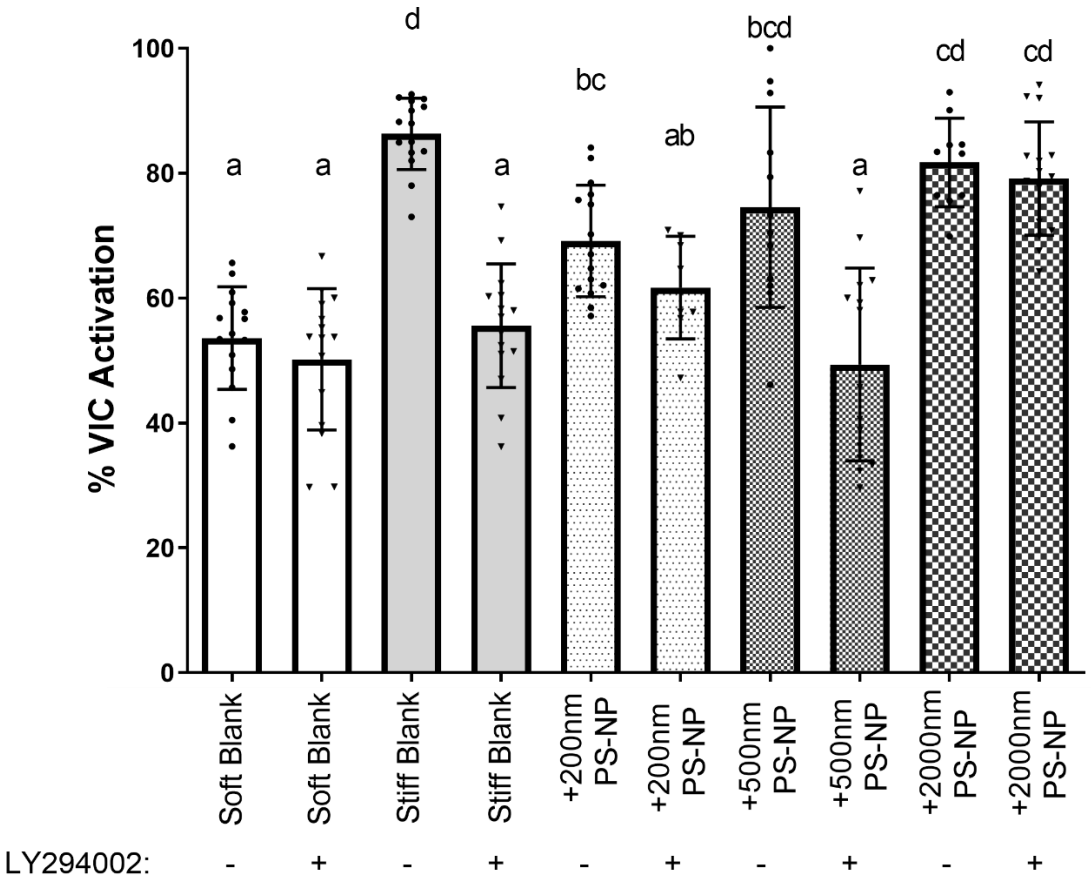
% VIC Activation
100
80
60
40
20
0
a
a
d
a
bc
ab
bcd
a
cd
cd
Soft Blank
Soft Blank
Stiff Blank
Stiff Blank
+200nm PS-NP
+200nm PS-NP
+500nm PS-NP
+500nm PS-NP
+2000nm PS-NP
+2000nm PS-NP
LY294002: - + - + - + - + - +

Figure 7: Male VIC focal adhesion size does not change on PS-NP gels when compared to the soft control. (A) Representative images of male VICs seeded on soft 4% PEG hydrogels containing 200 nm, 500 nm, or 2,000 nm PS-NPs. Stains: green = αSMA, magenta = paxillin, blue = nuclei. Scale bar = 100 μm. (B) Male VIC focal adhesion size in response to PS-NP gels. Sample size: $n = 3$ gels. Data were not statistically significant ($p < 0.05$).

A

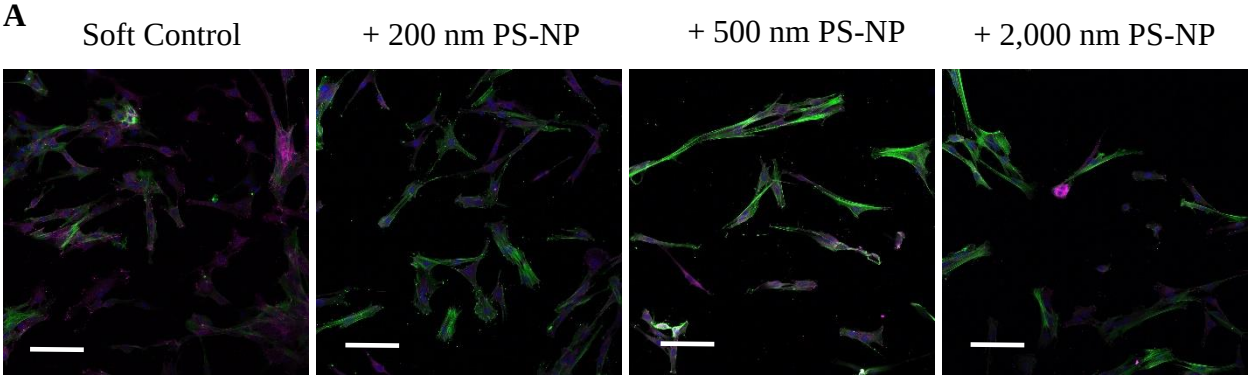

B

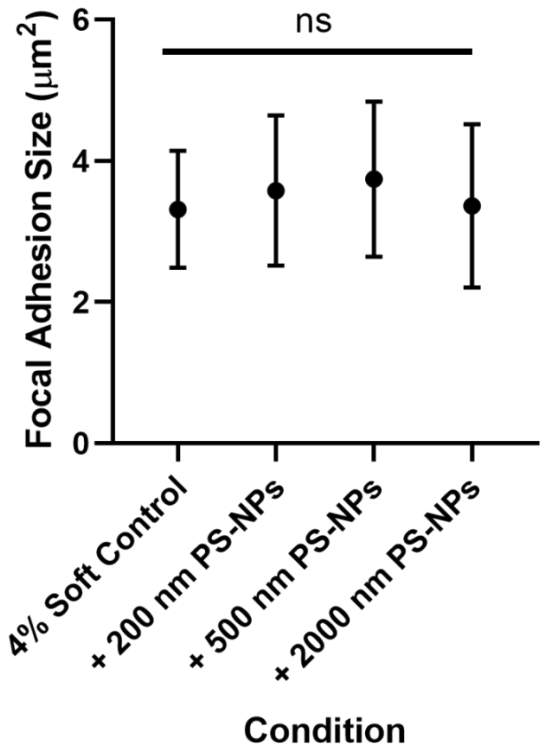

Figure 8: Plateau storage moduli (G') of PEG hydrogels with varying final concentrations (wt%) of PEG norbornene. Figure provided by Brian Aguado.

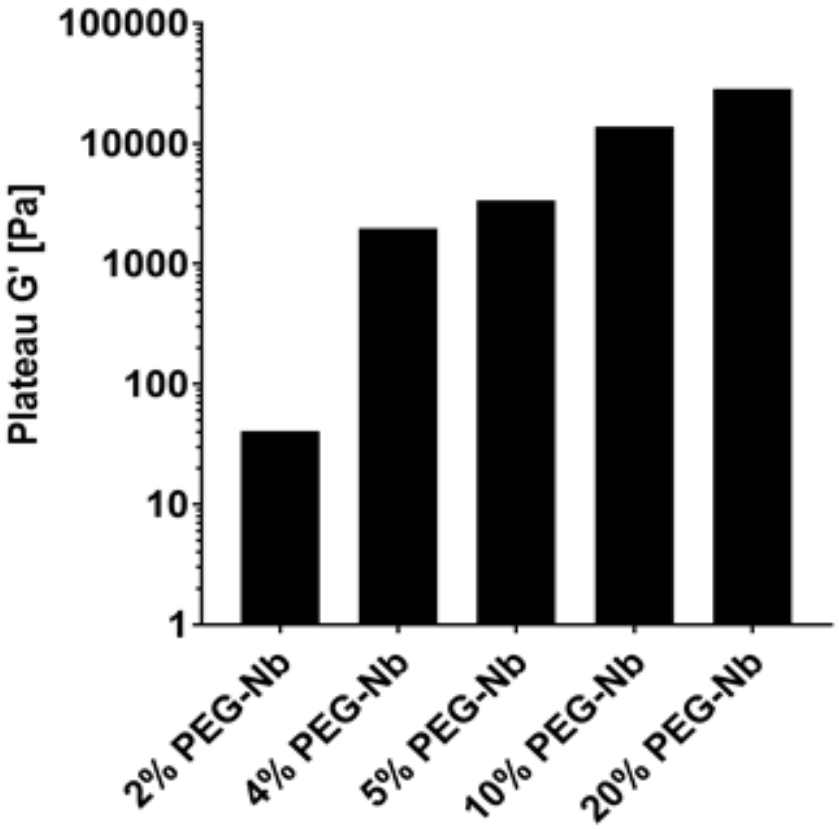

Figure 9: Particle Size distribution by Intensity of PEG nanogels. (A) 2% PEG nanogels. Z-average diameter = 391 nm. (B) 4% PEG nanogels. Z-average diameter = 307 nm. (C) 5% PEG nanogels. Z-average diameter = 329 nm. (D) 6% PEG nanogels. Z-average diameter = 203 nm. (E) 7% PEG nanogels. Z-average diameter = 378 nm. (F) 10% PEG nanogels. Z-average diameter = 380 nm. (G) 4% PEG nanogels without RGD. Z-average diameter = 325 nm. (H) 10% PEG nanogels without RGD. Z-average diameter = 318 nm.

A

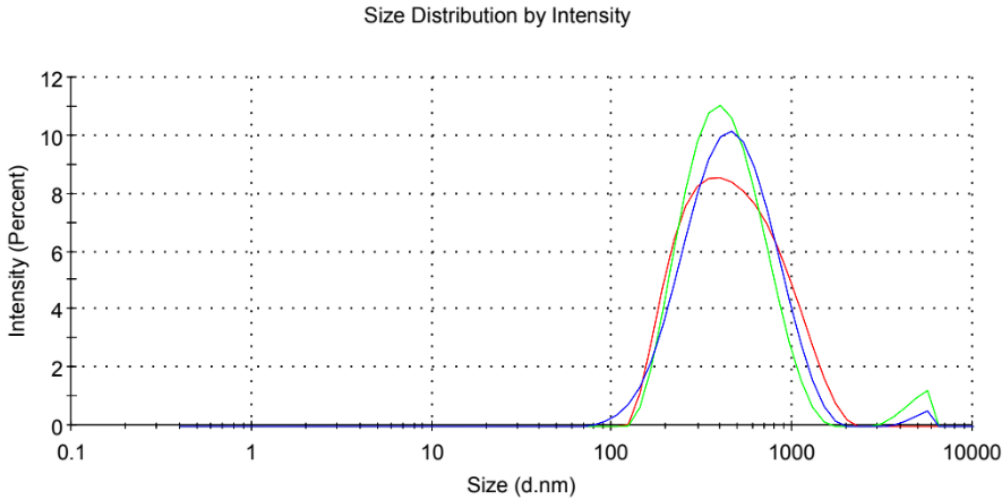

B

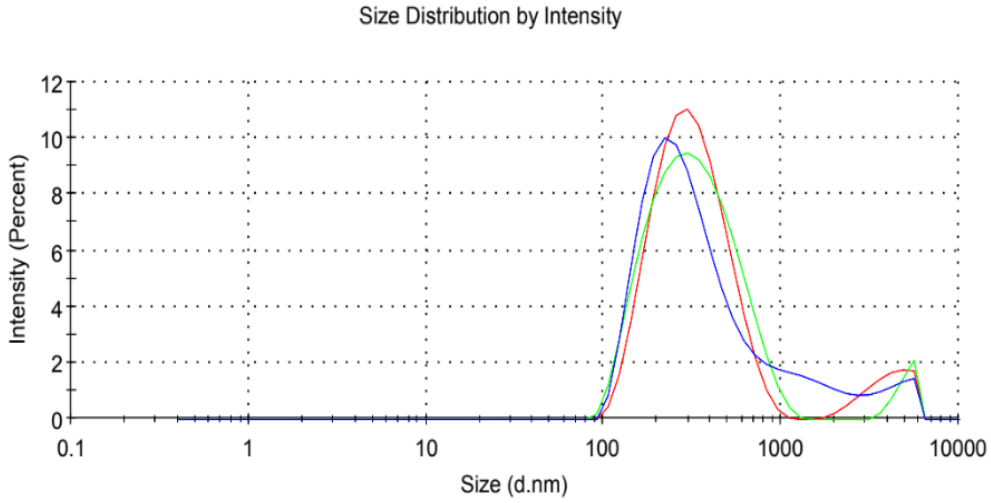

C

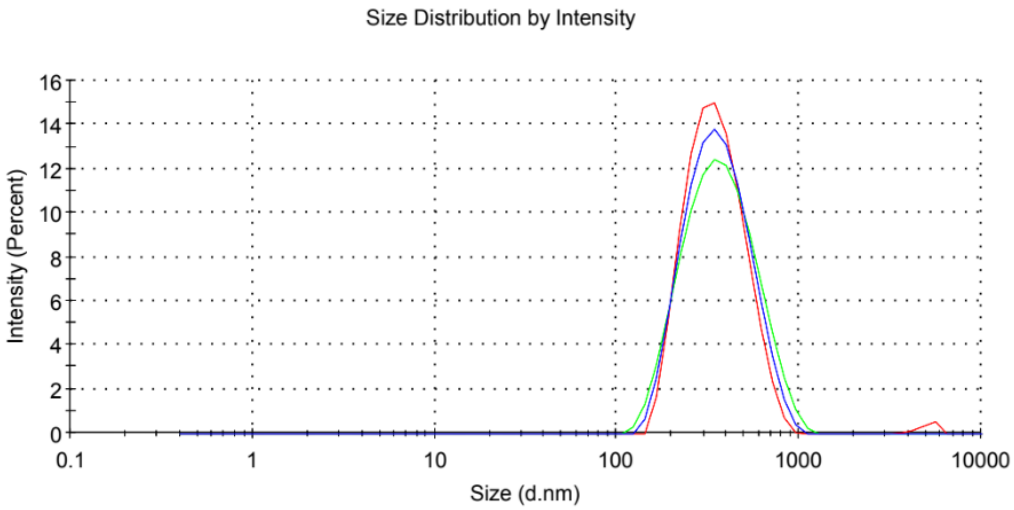
Size Distribution by Intensity
Intensity (Percent)
16
14
12
10
8
6
4
2
0
0.1
1
10
100
1000
10000
Size (d.nm)

D

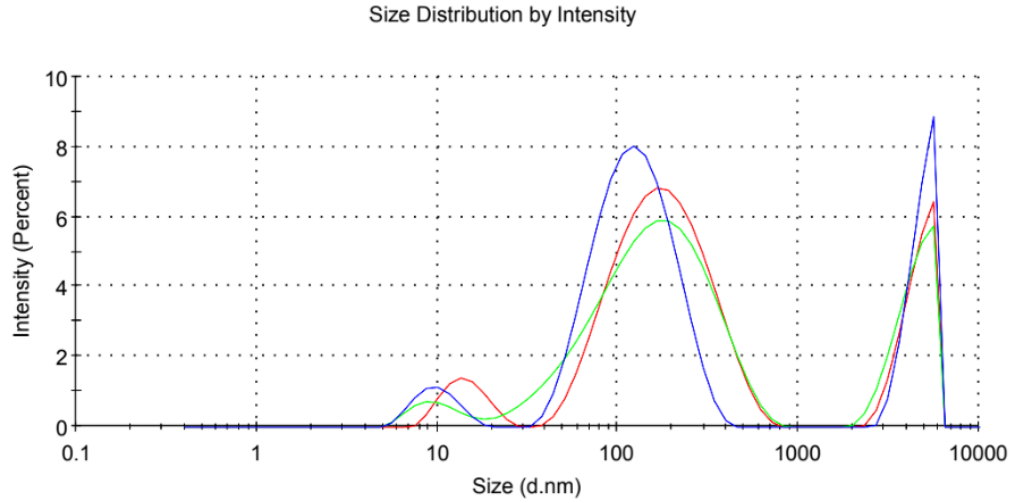
Size Distribution by Intensity
Intensity (Percent)
10
8
6
4
2
0
0.1
1
10
100
1000
10000
Size (d.nm)

E

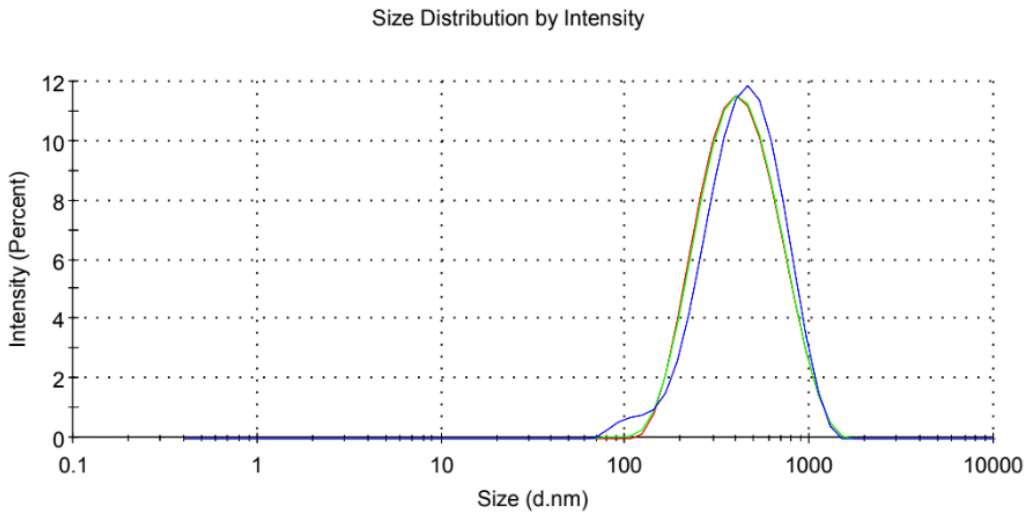
Size Distribution by Intensity
Intensity (Percent)
0
2
4
6
8
10
12
0.1
1
10
100
1000
10000
Size (d.nm)

F

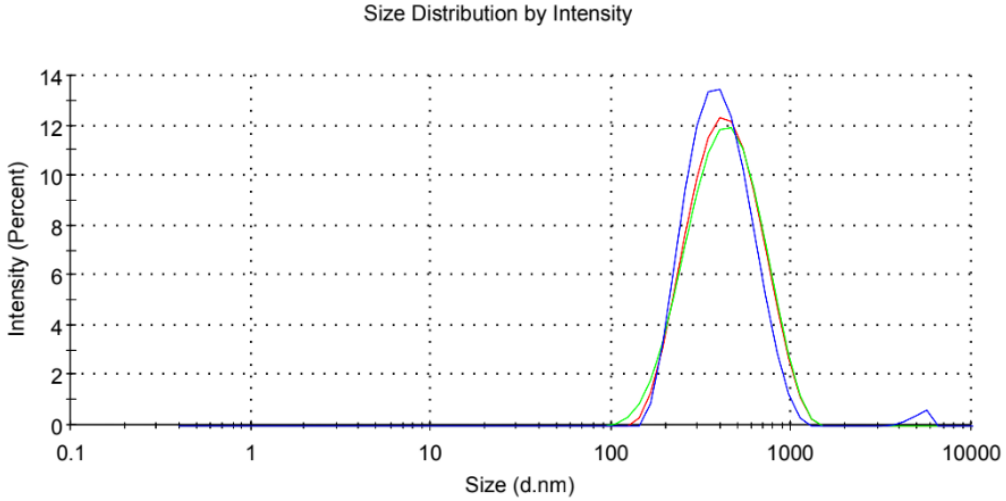
Size Distribution by Intensity
Intensity (Percent)
0
2
4
6
8
10
12
14
0.1
1
10
100
1000
10000
Size (d.nm)

G

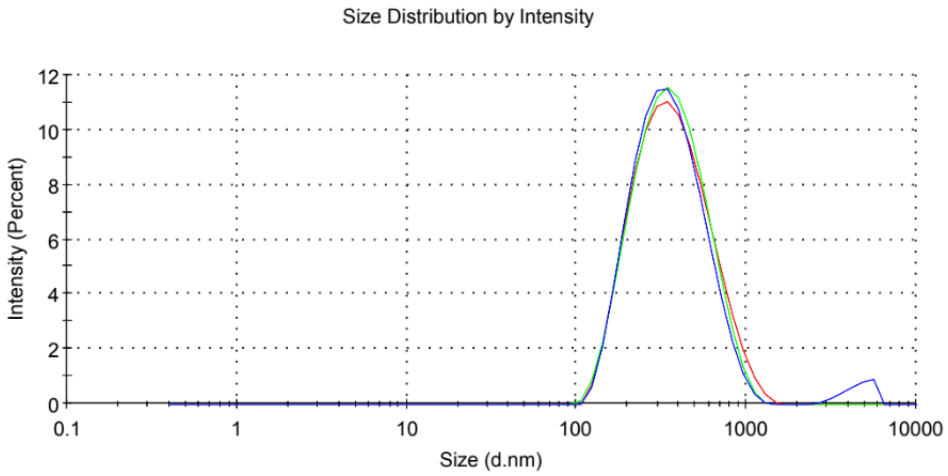
Size Distribution by Intensity
Intensity (Percent)
0
2
4
6
8
10
12
0.1
1
10
100
1000
10000
Size (d.nm)

H

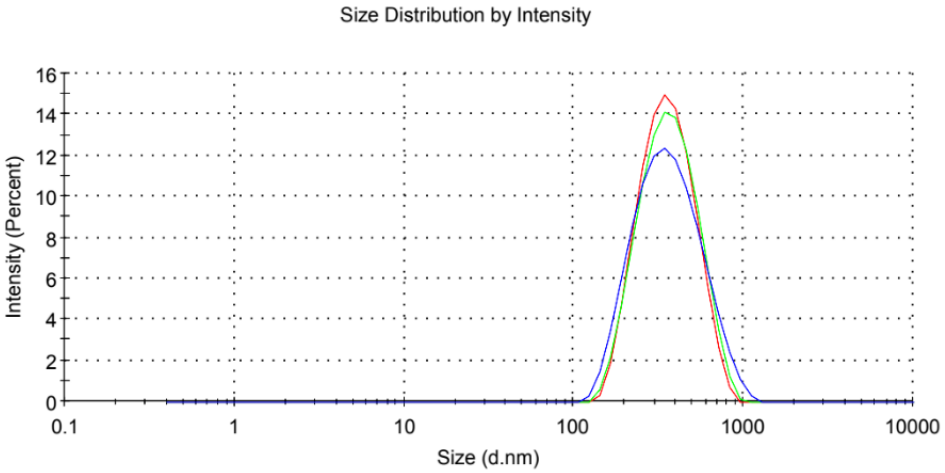
Size Distribution by Intensity
Intensity (Percent)
0
2
4
6
8
10
12
14
16
0.1
1
10
100
1000
10000
Size (d.nm)

Figure 10: Male VIC activation decreases in response to soft 4% PEG nanogels (NGs) embedded in stiff 10% PEG hydrogels. (A) Representative images of male VICs seeded on soft 4% PEG hydrogels, stiff 10% PEG hydrogels, and stiff 10% PEG hydrogels embedded with soft 4% PEG nanogels. Stains: green = αSMA, yellow = cytoplasm, blue = nuclei. Scale bar = 100 μm. (B) Male VIC activation on stiff 10% PEG hydrogels embedded with soft 4% PEG nanogels compared to controls. Sample size: n = 3 gels. Groups with different letters indicate statistical significance ($p < 0.05$).

A

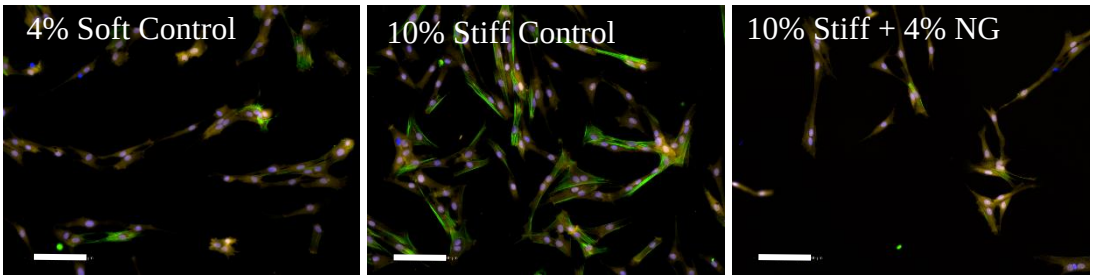

B

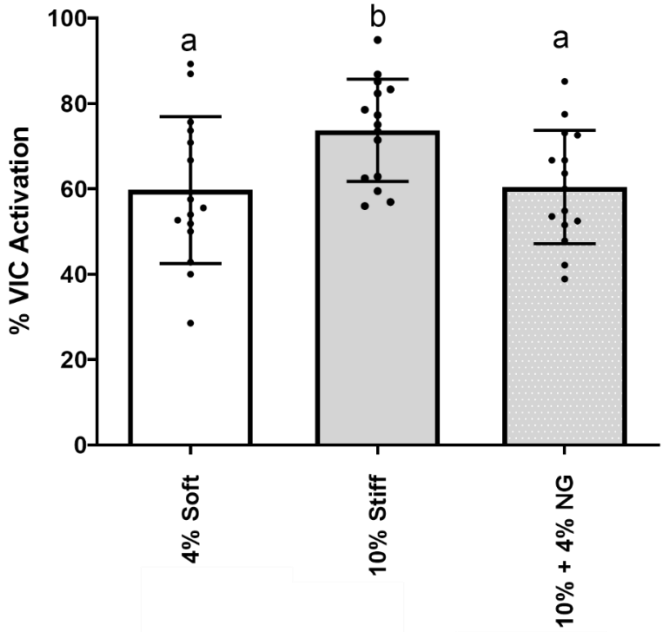

Figure 11: Female VICs remain activated on stiff 10% PEG hydrogels embedded with soft 4% PEG nanogels (NGs). (A) Representative images of female VICs seeded on soft 4% PEG hydrogels, stiff 10% PEG hydrogels, and stiff 10% PEG hydrogels embedded with soft 4% PEG nanogels (NGs). Stains: green = αSMA, red = cytoplasm, blue = nuclei. Scale bar = 100 μm. (B) Female VIC activation on stiff 10% PEG hydrogels embedded with soft 4% PEG nanogels compared to controls. Sample size: n = 3 gels. Groups with different letters indicate statistical significance ($p < 0.05$).

A

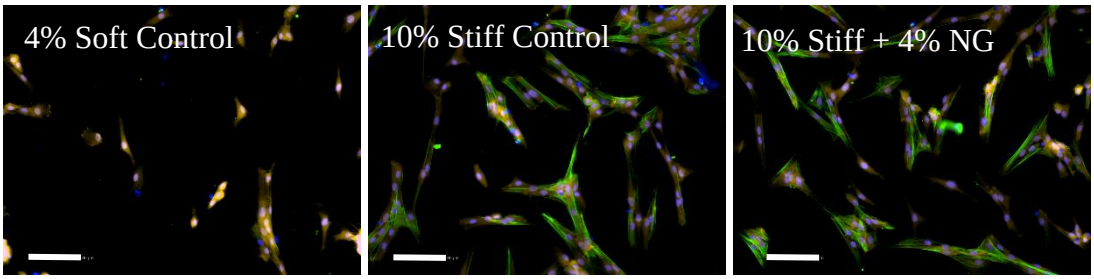

B

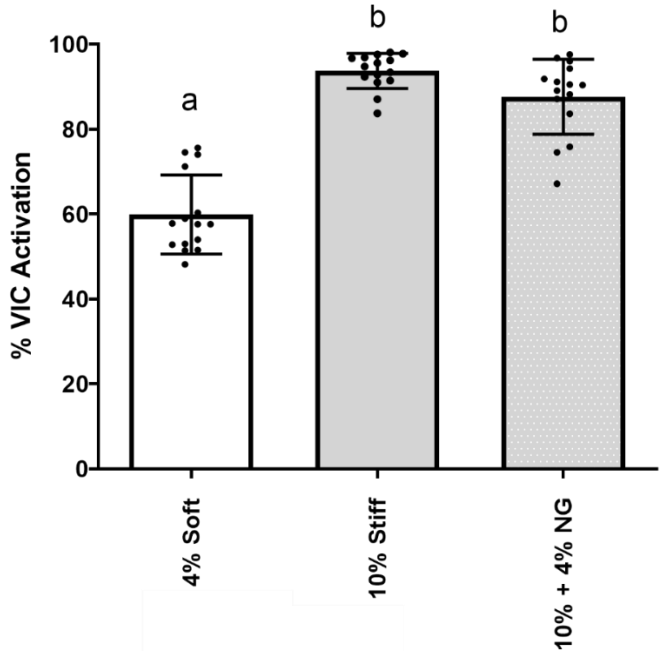

Figure 12: Male VIC activation increases as the stiffness of PEG nanogels (NGs) embedded in soft 4% PEG hydrogels increases. (A) Representative images of male VICs seeded on soft 4% PEG hydrogels embedded with 2, 4, 5, 6, 7, or 10 PEG wt% nanogels. Controls were blank 4% PEG hydrogels and 4% PEG hydrogels embedded with 200 nm PS-NPs. Stains: green = αSMA, blue = nuclei. Scale bar = 100 μm. (B) Male VIC activation on soft 4% PEG hydrogels embedded with PEG nanogels of varying stiffness. Sample size: n = 3 gels. Groups with different letters indicate statistical significance ($p < 0.05$).

A

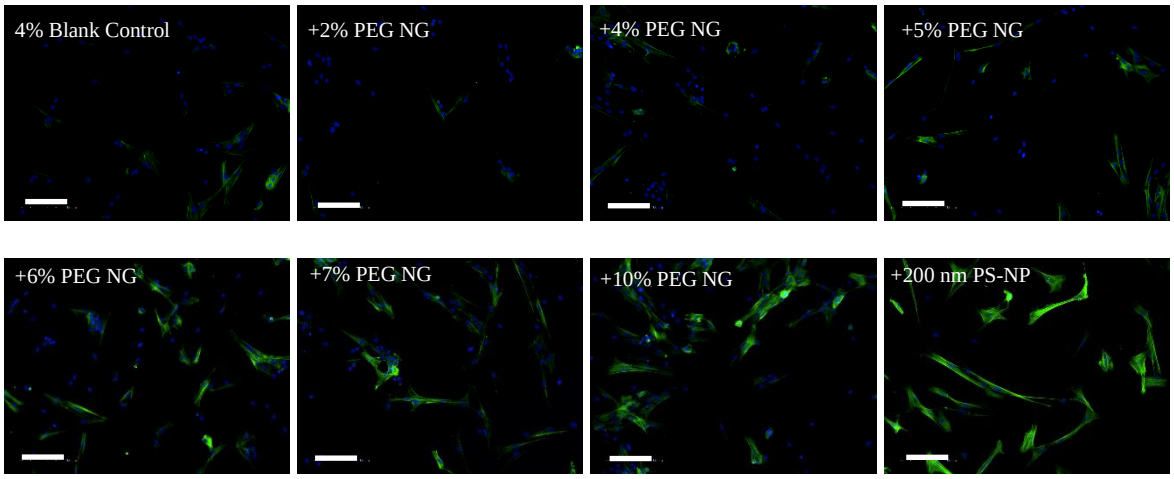

B

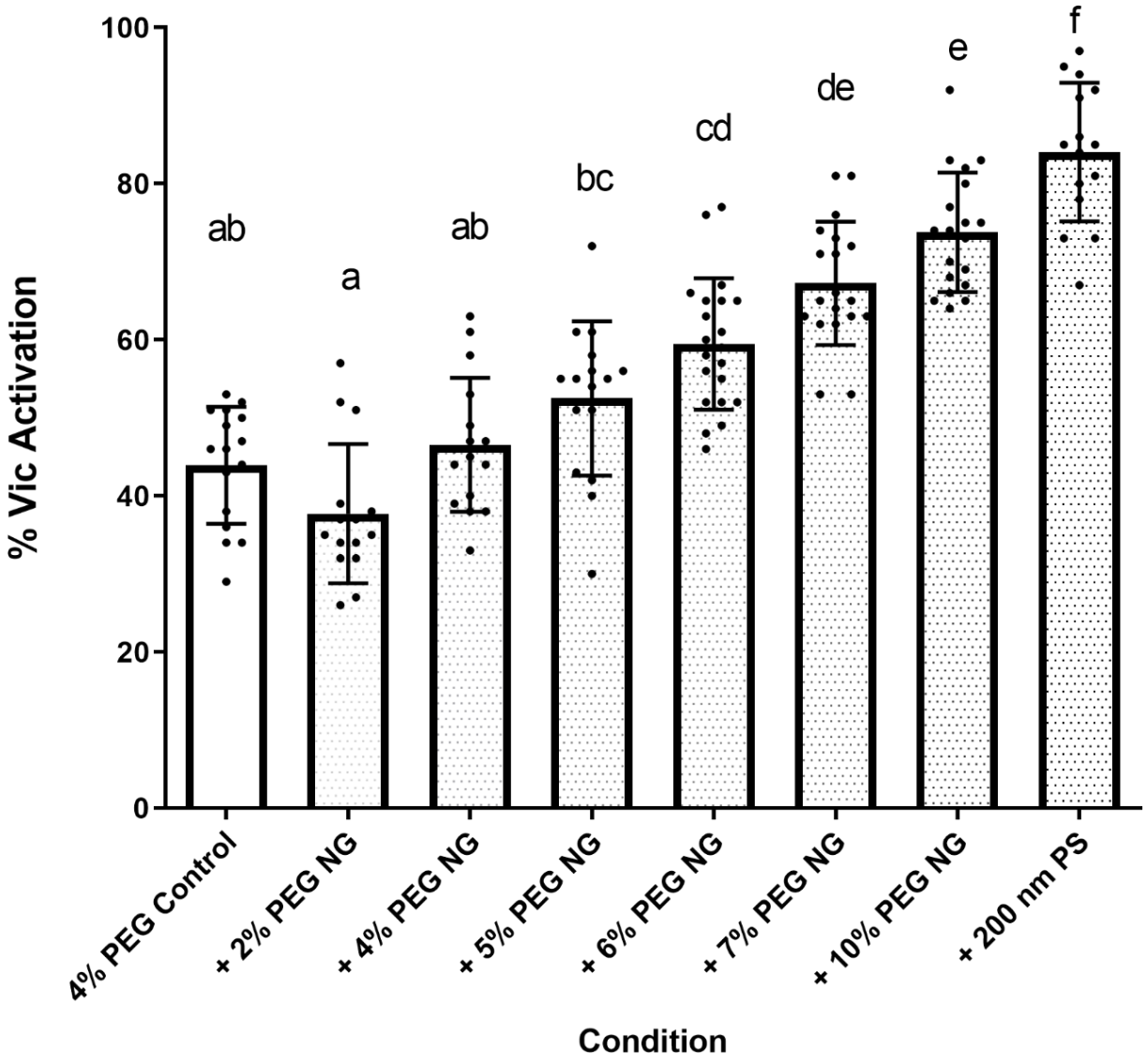
100
80
60
40
20
0
% Vic Activation
ab
a
ab
bc
cd
de
e
f
4% PEG Control
+ 2% PEG NG
+ 4% PEG NG
+ 5% PEG NG
+ 6% PEG NG
+ 7% PEG NG
+ 10% PEG NG
+ 200 nm PS
Condition

Figure 13: Male VIC activation decreases as the stiffness of PEG nanogels embedded in stiff 10% PEG hydrogels decreases. (A) Representative images of male VICs seeded on stiff 10% PEG hydrogels embedded with 2, 4, 5, 6, 7, or 10 PEG wt% nanogels. Controls were blank 10% PEG hydrogels and 10% PEG hydrogels embedded with 200 nm PS-NPs. Stains: green = αSMA, blue = nuclei. Scale bar = 100 μm. (B) Male VIC activation on stiff 10% PEG hydrogels embedded with PEG nanogels of varying stiffness. Sample size: n = 3 gels. Groups with different letters indicate statistical significance ($p < 0.05$).

A

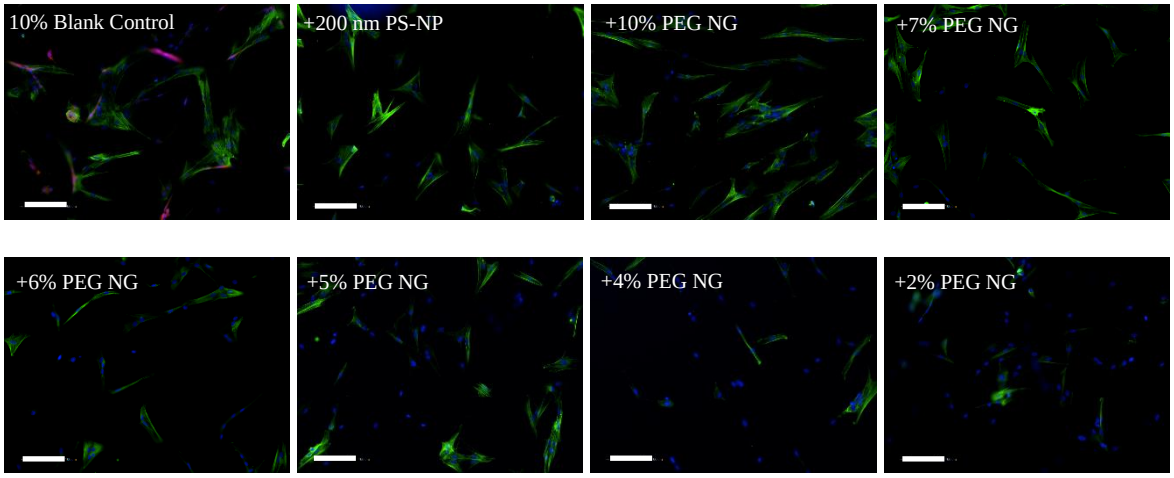

B

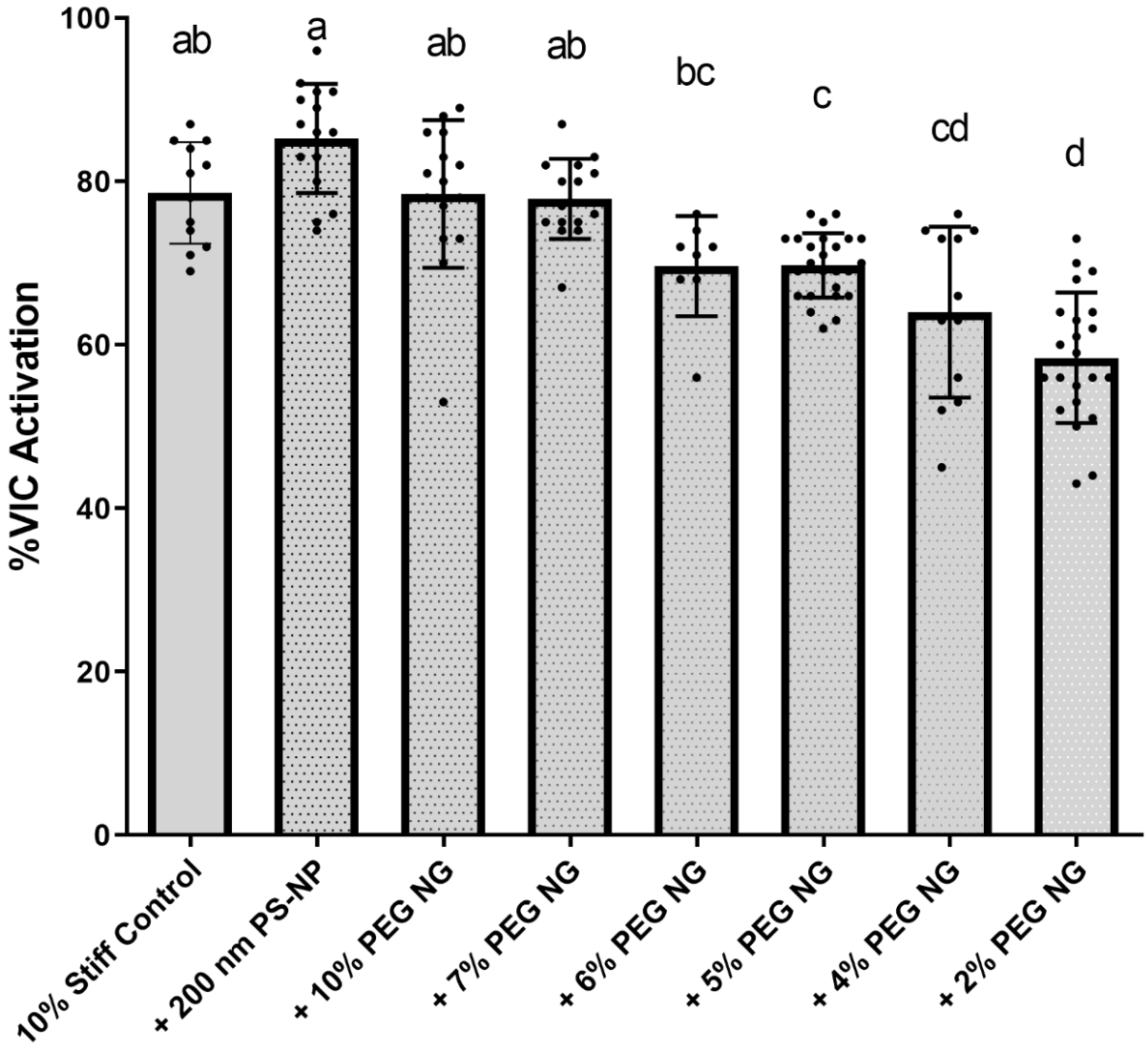
100
80
60
40
20
0
%VIC Activation
ab
a
ab
ab
bc
c
cd
d
10% Stiff Control
+ 200 nm PS-NP
+ 10% PEG NG
+ 7% PEG NG
+ 6% PEG NG
+ 5% PEG NG
+ 4% PEG NG
+ 2% PEG NG

Figure 14: Male and female VIC activation decreases when treated with soft 4% PEG nanogels and increases when treated with stiff 10% PEG nanogels. (A) Representative images of male VICs seeded on stiff 10% PEG hydrogels and treated with soft 4% PEG nanogels, seeded on soft 4% PEG hydrogels and treated with stiff 10% PEG nanogels, and seeded on soft 4% PEG hydrogels embedded with 200 nm PS-NPs and treated with soft 4% PEG nanogels. Controls not treated with nanogels. Stains: green = αSMA, blue = nuclei. Scale bar = 100 μm. (B) Representative images of female VICs seeded on stiff 10% PEG hydrogels and treated with soft 4% PEG nanogels, seeded on soft 4% PEG hydrogels and treated with stiff 10% PEG nanogels, and seeded on soft 4% PEG hydrogels embedded with 200 nm PS-NPs and treated with soft 4% PEG nanogels. Controls not treated with nanogels. Stains: green = αSMA, blue = nuclei. Scale bar = 100 μm. (C) Male VIC activation on soft 4% PEG hydrogels treated with stiff 10% PEG nanogels, on stiff 10% PEG hydrogels treated with soft 4% PEG nanogels at concentrations of 0.22 mg/μL or 0.43 mg/μL, and on soft 4% PEG hydrogels embedded with 200 nm PS-NPs and treated with soft 4% PEG nanogels at a concentration 0.43 mg/μL. (D) Male VIC activation on soft 4% PEG hydrogels treated with stiff 10% PEG nanogels, on stiff 10% PEG hydrogels treated with soft 4% PEG nanogels at concentrations of 0.22 mg/μL or 0.43 mg/μL, and on soft 4% PEG hydrogels embedded with 200 nm PS-NPs and treated with soft 4% PEG nanogels at a concentration 0.43 mg/μL. Sample size: $n = 3$ gels. Groups with different letters indicate statistical significance ($p < 0.05$).

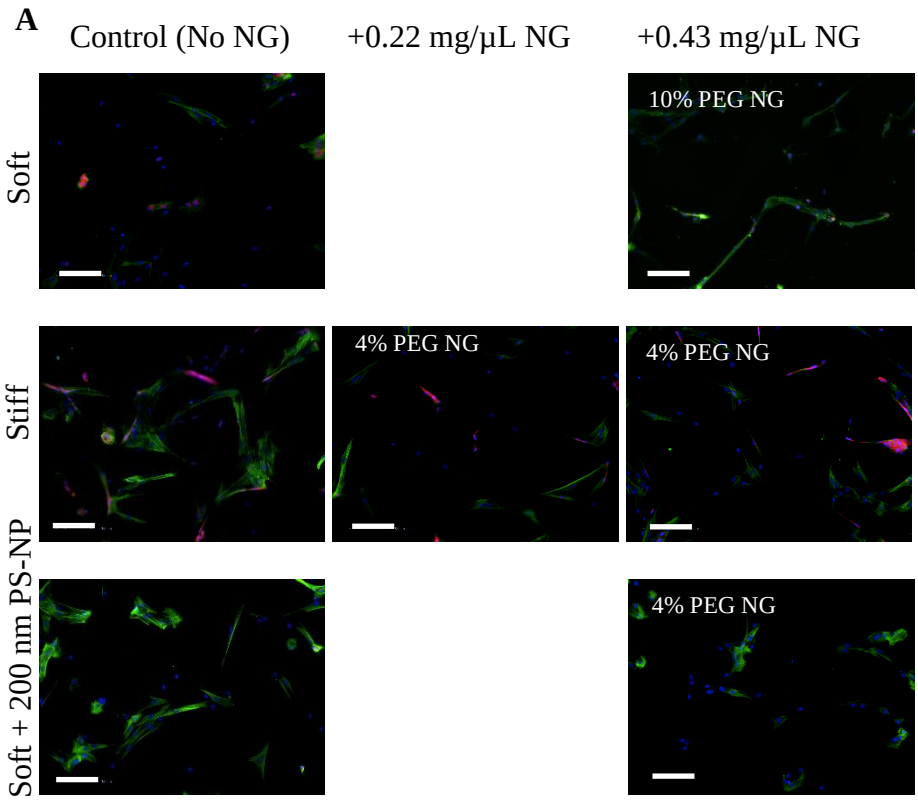
A
Control (No NG)
+0.22 mg/µL NG
+0.43 mg/µL NG
Soft
Stiff
Soft + 200 nm PS-NP
10% PEG NG
4% PEG NG
4% PEG NG
4% PEG NG
4% PEG NG

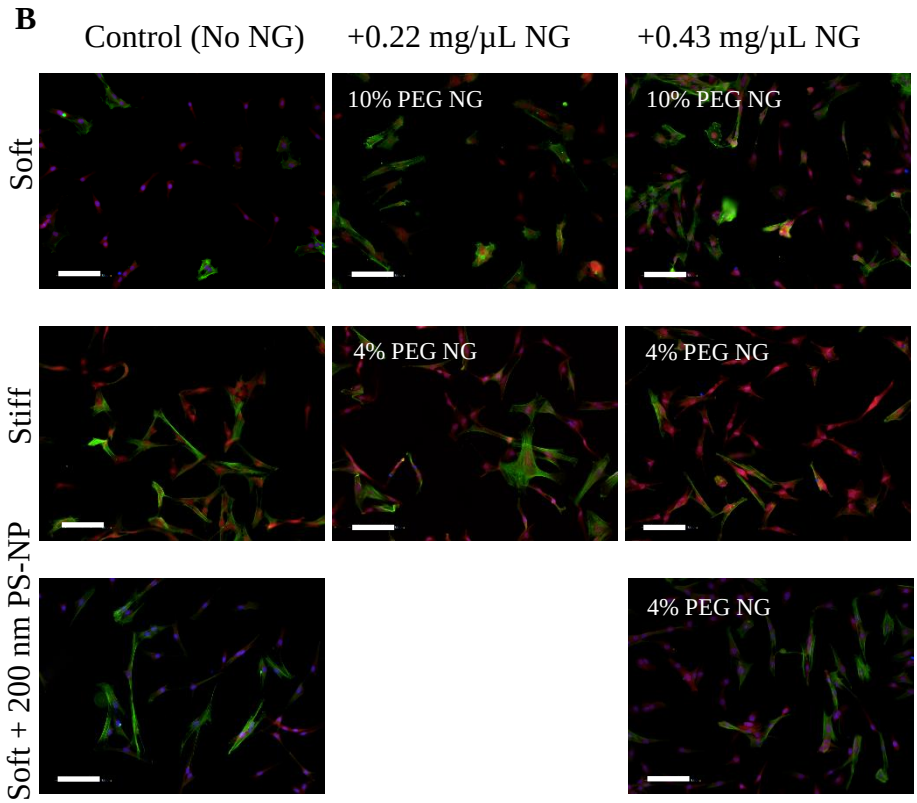
B
Control (No NG)
+0.22 mg/µL NG
+0.43 mg/µL NG
Soft
Stiff
Soft + 200 nm PS-NP
10% PEG NG
10% PEG NG
4% PEG NG
4% PEG NG
4% PEG NG

C

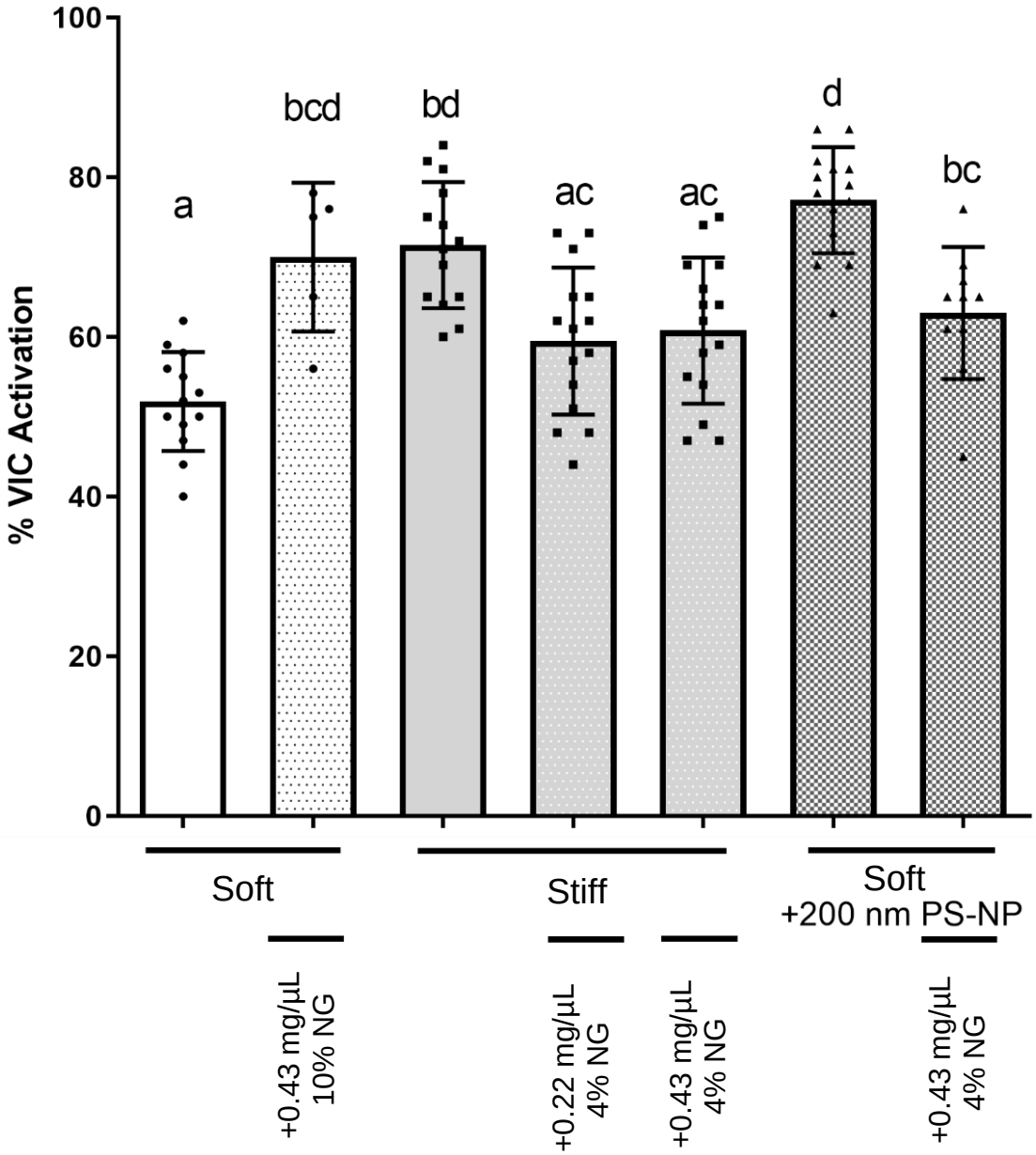
100
80
60
40
20
0
% VIC Activation
a
bcd
bd
ac
ac
d
bc
Soft
Stiff
Soft
+200 nm PS-NP
+0.43 mg/µL
10% NG
+0.22 mg/µL
4% NG
+0.43 mg/µL
4% NG
+0.43 mg/µL
4% NG

D

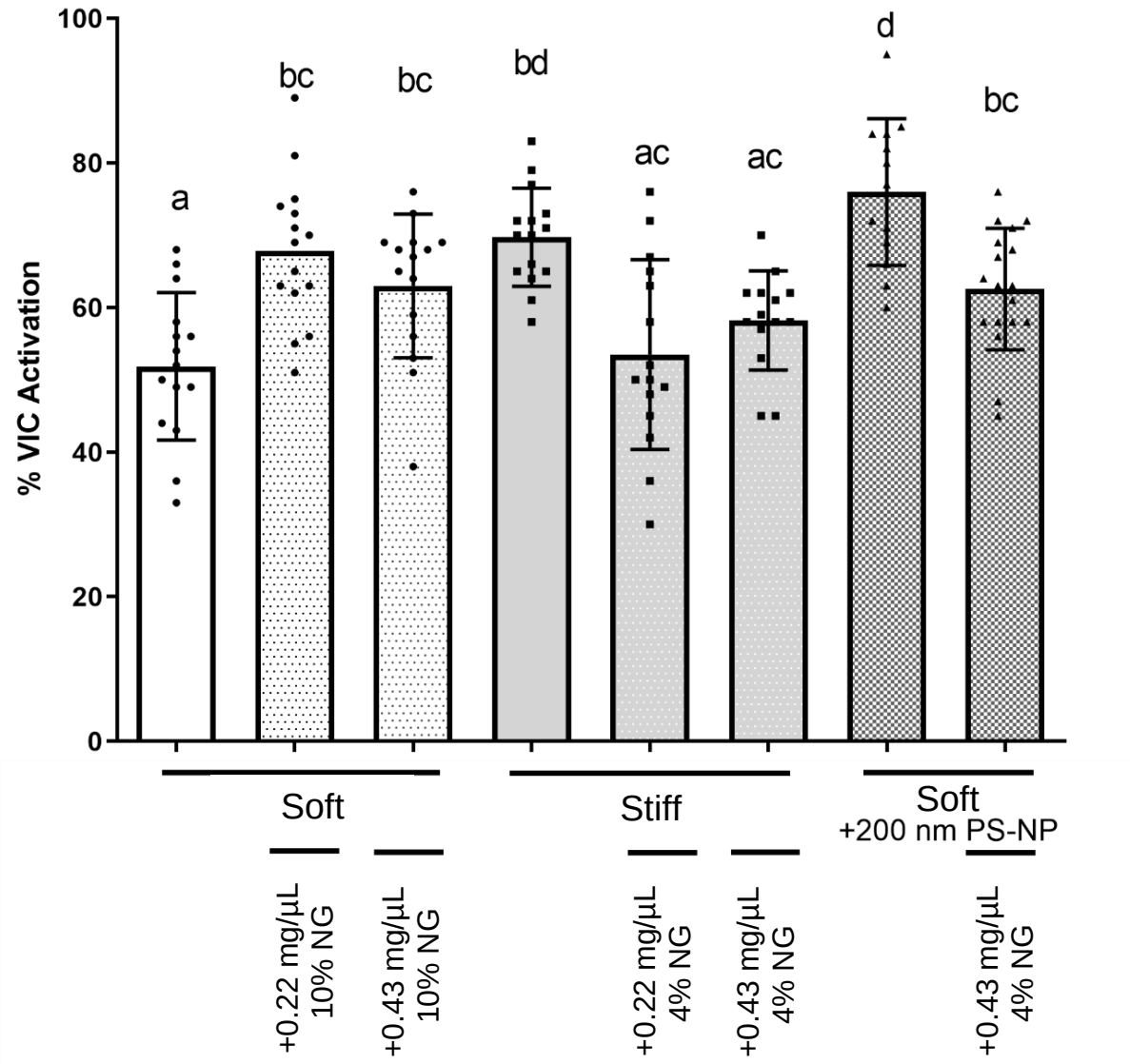
100
80
60
40
20
0
% VIC Activation
a
bc
bc
bd
ac
ac
d
bc
Soft
Stiff
Soft
+200 nm PS-NP
+0.22 mg/µL 10% NG
+0.43 mg/µL 10% NG
+0.22 mg/µL 4% NG
+0.43 mg/µL 4% NG
+0.43 mg/µL 4% NG

Acknowledgements

I would like to thank my thesis advisor Kristi Anseth, distinguished professor in the department of chemical and biological engineering at the University of Colorado Boulder, for welcoming me into her lab. Without her support, this thesis would not have been possible. I would also like to thank my thesis mentor Brian Aguado, postdoctoral researcher in the Anseth Lab, for volunteering to mentor me and allowing me to take part in his projects. His support and guidance have enriched my undergraduate experience and provided me with the tools to take on this challenging project. His thorough teaching style and high expectations of his mentees enriched my undergraduate research experience and provided me with the tools to work independently in the lab. I would also like to thank Dr. Carolyn Schoenbaum and my committee members Professor Jeffrey Cameron and Professor Joseph Jupille for their time in evaluating my thesis and providing guidance.

I would also like to acknowledge funding provided by the Nation Institute of Health Research Award. Furthermore, I would like to acknowledge the BioFrontiers Institute Advanced Light Microscopy Core. Laser scanning confocal microscopy was performed on a Nikon A1R microscope supported by NIST-CU Cooperative Agreement award number 70NANB15H226. I would also like to thank the VIC subgroup for welcoming me into their discussions and providing guidance for this project.

References

Aguado, B. A., Schuetze, K. B., Grim, J. C., Walker, C. J., Tan, A., Cox, A. C., Taylor, M. R. G., McKinsey, T. A., & Anseth, K. S. (2019). Transcatheter aortic valve replacements alter circulating serum factors that mediate myofibroblast activation of valvular interstitial cells.

Anselmo, A. C., Zhang, M., Kumar, S., Vogus, D. R., Menegatti, S., Helgeson, M. E., & Mitragotri, S. (2015). Elasticity of nanoparticles influences their blood circulation, phagocytosis, endocytosis, and targeting. *ACS Nano, 9*, 3169-3177. https://doi.org/10.1021/acsnano.5b00147

Bertazzo, S., Gentleman, E., Cloyd, K. L., Chester, A. H., Yacoub, M. H., & Stevens, M. M. (2013). Nano-analytical electron microscopy reveals fundamental insights into human cardiovascular tissue calcification. *Nature Materials, 12*, 576-583. https://doi.org/10.1038/NMAT3627

Carabello, B. A. & Paulus, W. J. (2009). Aortic Stenosis. *Lancet, 373,* 956-966. https://doi.org/10.1016/S0140- 6736(09)60211-7

Chen, C. S., Mrksich, M., Huang, S., Whitesides, G. M., & Ingber, D. E. (1997). Geometric control of cell life and death. *Science*, *276*, 1425-1428. https://doi.org/10.1126/science.276.5317.1425

Chi-Rosso, G., Gotwals, P. J., Yang, J., Ling, L., Jiang, K., Chao, B., Baker, D. P., Burkly, L. C. Fawell, S. E., & Koteliansky, V. E. (1997). Fibronectin type III repeats mediate RGD-independent adhesion and signaling through activated β1 integrins. *The Journal of Biological Chemistry, 272*(50), 31447-31452.

Cramariuc, D., Rogge, B. P., Lonnebakken, M. T., Boman, K., Bahlmann, E., Gohlke-Barwolf, C., Chambers, J. B., Pedersen, T. R., & Gerdts, E. (2014). Sex differences in cardiovascular outcome during progression of aortic valve stenosis. *Heart, 101*(3), 209-214. https://doi.org/10.1136/heartjnl-2014-306078

Cushing, M. C., Liao, J. T., & Anseth, K. S. (2005). Activation of valvular interstitial cells is mediated by transforming growth factor-beta1 interactions with matrix molecules. *Matrix Biology, 24*(6). 428-437. https://doi.org/10.1016/j.matbio.2005.06.007

Demer, L. L., & Tintut, Y. (2008). Vascular calcification: pathobiology of a multifaceted disease. *Circulation, 117*(22), 2938-2948. https://doi.org/10.1161/CIRCULATIONAHA.107.743161

Faggiano, P., Antonini-Canterin, F., Baldessin, F., Lorusso, R., D'Aloia, A., & Dei Cas, L. (2006). Epidemiology and cardiovascular risk factors of aortic stenosis. *Cardiovasc Ultrasound, 4*(27). https://doi.org/10.1186/1476-7120-4-27

Fairbanks, B. D., Schwartz, M. P., Halevi, A. E., Nuttelman, C. R., Bowman, C. N., & Anseth K. S. (2009). A versatile synthetic extracellular matrix mimic via thiol-norbornene photopolymerization. *Adv Mater, 21*(48), 5005-5010. https://doi.org/10.1002/adma.200901808

Garcia-Hevia, L., Valiente, R., Martin-Rodriguez, R., Renero-Lecuna, C., Gonzalez, J., Rodriguez-Fernandez, L., Aguado, F., Villegas, J. C., & Fanarraga, M. L. (2016). Nano-ZnO leads to tubulin macrotube assembly and actin bundling, triggering cytoskeletal catastrophe and cell necrosis. *Nanoscale, 8*(21), 10963-10973. https://doi.org/10.1039/c6nr00391e

Goffin, J. M., Pittet, P., Csucs, G., Lussi, J. W., Meister, J. J., & Hinz, B. (2006). Focal adhesion size controls tension-dependent recruitment of alpha-smooth muscle actin to stress fibers. *The Journal of Cell Biology, 172*(2), 259-268. https://doi.org/10.1083/jcb.200506179

Gould, S.T., Darling, N. J., & Anseth, K. S. (2012). Small peptide functionalized thiol-ene hydrogels as culture substrates for understanding valvular interstitial cell activation and de novo tissue deposition. *Acta Biomater 8*, 3201-320. https://doi.org/10.1016/j.actbio.2012.05.009

Gupta, A. K., Gupta, M., Yarwood, S. J., & Curtis, A. S. (2004). Effect of cellular uptake of gelatin nanoparticles on adhesion, morphology and cytoskeleton organization of human fibroblasts. *Journal of Controlled Release, 95*(2), 197-207. https://doi.org/10.1016/j.jconrel.2003.11.006

Leon, M. B., Smith, C. R., Mack, M., Miller, C., Moses, J. W., Svensson, L. G., Tuzcu, M., Webb, J. G., Fontana, G. P., Makkar, R. R., Brown., D. L., & Block, P. C. (2010). Transcatheter aortic-valve implantation for aortic stenosis in patients who cannot undergo surgery. *The New England Journal of Medicine, 363*, 1597-1607. https://doi.org/10.1056/NEJMoa1008232

Li, B., Xie, J., Yuan, Z., Jain, P., Lin, X., Wu, K., & Jiang, S., (2018). Mitigation of inflammatory immune responses with hydrophilic nanoparticles. *Angewandte Chemie International Edition, 57*, 4527-4531. https://doi.org/10.1002/anie.201710068

Liu, W., Zhou, X., Mao, Z., Yu, D., Wang, B., & Gao, C. (2012). Uptake of hydrogel particles with different stiffness and its influence on HepG2 cell functions. *Soft Matter, 8*, 9235-9245. https://doi.org/10.1039/c2sm26001h

Ma, H., Killaars, A. R., DelRio, F. W., Yang, C., & Anseth, K., S. (2017). Myofibroblastic activation of valvular interstitial cells is modulated by spatial variations in matrix elasticity and its organization. *Biomaterials, 131*, 131-144. https://doi.org/10.1016/j.biomaterials.2017.03.040

Mabry, K. M., Lawrence, R. L., & Anseth, K. S. (2015). Dynamic stiffening of poly(ethylene glycol)-base hydrogels to direct valvular interstitial cell phenotype in a three-dimensional environment. *Biomaterials, 49,* 47-56. https://doi.org/10.1016/j.biomaterials.2015.01.047

Mabry, K. M., Payne, S. Z., & Anseth, K. S. (2016). Microarray analyses to quantify advantages of 2D and 3D hydrogel culture systems in maintaining the native valvular interstitial cell phenotype. *Biomaterials, 74*, 31-41. https://doi.org/10.1016/j.biomaterials.2015.09.035

Marquis-Gravel, G., Redfors, B., Leon, M. B., & Genereux, P. (2016). Medical treatment of aortic stenosis. *Circulation, 134*(22), 1766-1784. https://doi.org/10.1161/CIRCULATIONAHA.116.023997

McCoy, C. M., Nicholas, D. Q., Masters, K. S. (2012). Sex-related differences in gene expression by porcine aortic valvular interstitial cells. *PLoSONE, 7(7),* e39980. https://doi.org/10.1371/journal.pone.0039980

Nel, A. E., Madler, L., Velegol, D., Xia, T., Hoek, E. M. V., Somasundaran, P., Klaessig, F., Castranova, V., & Thompson, M. (2009). Understanding biophysiochemical interactions at the nano-bio interface. *Nature Materials, 8,* 543-557. https://doi.org/10.1038/NMAT2442

Niu, Y. & Zhao, Y. (2018). A microfluidic device for mechanical profiling of hydrogel microparticles. Presented at Solid-State Sensors, Actuators and Microsystems Workshop Hilton Head, 7-10. https://doi.org/10.31438/trf.hh2018.3

Osnabrugge, R. L., Mylotte, D., Head, S. J. Van Mieghem, N. M., Nkomo, V. T. LeReun, C. M., Bogers, A. J., Piazza, N., & Kppetein, A. P. (2013) Aortic stenosis in the elderly: disease prevalence and number of candidates for transcatheter aortic valve replacement: a meta-analysis and modeling study. *J Am Coll Cardiol, 62*, 1002-1012. https://10.1016/j.jacc.2013.05.015

Pati, R., Das, I., Mehta, R. K., Sahu, R., & Sonawane, A. (2016). Zinc-oxide nanoparticles exhibit genotoxic, clastogenic, cytotoxic and actin depolymerization effects by inducing oxidative stress responses in macrophages and adult mice. *Toxicological Sciences, 150*(2), 454-472. https://doi.org/10.1093/toxsci/kfw010

Pernodet, N., Fang, X., Sun, Y., Bakhtina, A., Ramakrishnan, A., Sokolov, J., Ulman, A., & Rafailovich, M. (2006). Adverse effects of citrate/gold nanoparticles on human dermal fibroblasts. *Small, 2*(6), 766. https://doi.org/10.1002/smll.200500492

Rajamannan, N. M., Subramaniam, M., Rickard, D., Stock, S. R., Donovan, J., Springett, M., Orszulak, T., Fullerton, D. A., Tajik, A. J., Bonow, R. O., & Spelsberg, T. (2003). Human aortic valve calcification is associated with an osteoblast phenotype. *Circulation, 107*(17), 2181-2184. https://doi.org/10.1161/01.CIR.0000070591.21548.69

Schlotter, F., Halu, A., Goto, S., Blaser, M. C., Body, S. C., Lee, L. H., Higashi, H., DeLaughter, D. M., Hutcheson, J. D., Vyas, P., Pham, T., Rogers, M. A., Sharma, A., Seidman, C. E., Loscalzo, J., Seidman, J. G., Aikawa, M., Singh, S. A. & Aikawa, E. (2018). Spatiotemporal multi-omics mapping generates a molecular atlas of the aortic valve and reveals networks driving disease. *Circulation, 138,* 377-393. https://doi.org/10.1161/CIRCULATIONAHA.117.032291

Septiadi, D., Crippa, F., Moore, T. L., Rothen-Rutishauser, B., & Petri-Fink, A. (2018). Nanoparticle-cell interaction: a cell mechanics perspective. *Advanced Materials, 30,* 1704463-1704463. https://doi.org/10.1002/adma.201704463

Shang, L., Nienhaus, K., & Nienhaus, G. U. (2014). Engineered nanoparticles interacting with cells: size matters. *Journal of Nanobiotechnology, 12*(5). https://doi.org/10.1186/1477-3155-12-5

Simard, L., Cote, N., Dagenais, F., Mathieu, P., Couture, C., Trahan, S., Bosse, Y., Mohammadi, S., Page, S., Joubert, P., & Clavel, M. (2017). Sex-related discordance between aortic valve calcification and hemodynamic severity of aortic stenosis. *Clinical Track, 120,* 681-691. https://doi.org/10.1161/CIRCRESAHA.116.309306

Utku, H., Ozdil, B., & Pesen-Okvur, D. (2014). Step-by-step quantitative analysis of focal adhesions. *MethodsX*, 1, 56-59. https://doi.org/10.1016/j.mex.2014.06.004

Vieira, L. F., Lins, M. P., Viana, I. M., Santos, J. E., Smaniotto, S., & Reis, M. D. (2017). Metallic nanoparticles reduce the migration of human fibroblasts in vitro. *Nanoscale Research Letters, 12*(1), 200. https://doi.org/10.1186/s11671-017-1982-3

Wang, H., Tibbitt, M. W., Langer, S. J., Leinwand, L. A., & Anseth, K. S. (2013). Hydrogels preserve native phenotypes of valvular fibroblasts through an elasticity-regulated PI3K/AKT pathway. *PNAS, 110*(48), 19336-19341. https://www.pnas.org/cgi/doi/10.1073/pnas.1306369110

Wang, Y., Chen, S., Deng, C., Li, F., Wang, Y., Hu, X., Shi, F., & Dong, N. (2015). MicroRNA-204 targets Runx2 to attenuate BMP-2-induced osteoblast differentiation of human aortic valve interstitial cells. *Journal of Cardiovascular Pharmacology, 66*(1), 63-71. https://doi.org/10.1097/FJC.0000000000000244

Weiss, R. M., Miller, J. D., & Heistad, D. D. (2013). Fibrocalcific aortic valve disease: opportunity to understand disease mechanisms using mouse models. *Circulation Research, 113,* 209-222. https://doi.org/10.1161/CIRCRESAHA.113.300153

Weska, R. F., Aimoli, C. G., Nogueira, G. M., Leirner, A. A., Maizato, M. J. S., Higa, O. Z., Polakievicz, B., Pitombo, R. N. M., & Beppu, M. M. (2010). Natural and prosthetic heart valve calcification: morphology and chemical composition characterization. *Artificial Organs 4*(4), 1525-1594. https://doi.org/10.1111/j.1525-1594.2009.00858.x

Wu, X., Tan, Y., Mao, H., & Zhang, M. (2010). Toxic effects of iron oxide nanoparticles on human umbilical vein endothelial cells. *International Journal of Nanomedicine, 5,* 385-399.

Yang, C., DelRio, F. W., Ma, H., Killaars, A. R., Basta, L. P., Kyburz, K. A., & Anseth, K. S. (2016). Spatially patterned matrix elasticity directs stem cell fate. *PNAS, 113*(31), E4439-E4445. https://doi.org/10.1073/pnas.1609731113

Zamir, E., Katz, M., Posen, Y., Erez, N., Yamada, K. M., Katz, B. Z., & Geiger, B. Dynamics and segregation of cell-matrix adhesions in cultured fibroblasts. (2000). *Nature Cell Biology, 2*(4), 191-196. https://doi.org/10.1038/35008607